Integrated Ocean Drilling Program
Expedition 348 Preliminary Report

NanTroSEIZE Stage 3:
NanTroSEIZE plate boundary deep riser 3

13 September 2013–29 January 2014

Expedition 348 Scientists and Scientific Participants

Published by
Integrated Ocean Drilling Program Management International, Inc.,
for the Integrated Ocean Drilling Program

Publisher's notes

Distribution:
Electronic copies of this series may be obtained from the Integrated Ocean Drilling Program (IODP) Scientific Publications homepage on the World Wide Web at **www.iodp.org/scientific-publications/.**

This publication was prepared by the Japanese Implementing Organization, Center for Deep Earth Exploration (CDEX) at the Japan Agency for Marine-Earth Science and Technology (JAMSTEC), as an account of work performed under the international Integrated Ocean Drilling Program (IODP), which is managed by IODP Management International (IODP-MI), Inc. Funding for the program is provided by the following agencies:

National Science Foundation (NSF), United States

Ministry of Education, Culture, Sports, Science and Technology (MEXT), Japan

European Consortium for Ocean Research Drilling (ECORD)

Ministry of Science and Technology (MOST), People's Republic of China

Korea Institute of Geoscience and Mineral Resources (KIGAM)

Australian Research Council (ARC) and GNS Science (New Zealand), Australian/New Zealand Consortium

Ministry of Earth Sciences (MoES), India

Coordination for Improvement of Higher Education Personnel, Brazil

Disclaimer

Copyright

Citation:
Expedition 348 Scientists and Scientific Participants, 2014. NanTroSEIZE Stage 3: NanTroSEIZE plate boundary deep riser 3. *IODP Prel. Rept.,* 348. doi:10.2204/iodp.pr.348.2014

August 2014

Expedition 348 participants

Expedition 348 scientists

Harold Tobin
Co-Chief Scientist
Department of Geoscience
University of Wisconsin-Madison
1215 West Dayton Street
Madison WI 53706
USA
htobin@wisc.edu

Takehiro Hirose
Co-Chief Scientist
Kochi Institute for Core Sample Research
Japan Agency for Marine-Earth Science and Technology
200 Monobe Otsu, Nankoku City
Kochi 783-8502
Japan
hiroset@jamstec.go.jp

Demian Saffer
Co-Chief Scientist
Department of Geosciences
The Pennsylvania State University
534 Deike Building
University Park PA 16802
USA
dms45@psu.edu

Sean Toczko
Lead Expedition Project Manager
Center for Deep Earth Exploration
Japan Agency for Marine-Earth Science and Technology
3173-25 Showa-machi
Kanazawa-ku, Yokohama
Kanagawa 236-0001
Japan
sean@jamstec.go.jp

Lena Maeda
Expedition Project Manager
Center for Deep Earth Exploration
Japan Agency for Marine-Earth Science and Technology
3173-25 Showa-machi
Kanazawa-ku, Yokohama
Kanagawa 236-0001
Japan
maedal@jamtec.go.jp

Yusuke Kubo
Expedition Project Manager
Center for Deep Earth Exploration
Japan Agency for Marine-Earth Science and Technology
3173-25 Showa-machi
Kanazawa-ku, Yokohama
Kanagawa 236-0001
Japan
kuboy@jamstec.go.jp

Yoshinori Sanada
Lead Logging Staff Scientist
Center for Deep Earth Exploration
Japan Agency for Marine-Earth Science and Technology
3173-25 Showa-machi
Kanazawa-ku, Yokohama
Kanagawa 236-0001
Japan
sanada@jamstec.go.jp

Yukari Kido
Logging Staff Scientist
Center for Deep Earth Exploration
Japan Agency for Marine-Earth Science and Technology
3173-25 Showa-machi
Kanazawa-ku, Yokohama
Kanagawa 236-0001
Japan
ykido@jamstec.go.jp

Yohei Hamada
Logging Staff Scientist
Institute for Research on Earth Evolution
Japan Agency for Marine-Earth Science and Technology
2-15 Natsushima-Cho, Yokosuka
Kanagawa 237-0061
Japan
yhamada@jamstec.go.jp

Brian Boston
Downhole Logging Specialist
Department of Geology and Geophysics
University of Hawaii
1680 East-West Road
Honolulu HI 96822
USA
bboston@hawaii.edu

Aisling Broderick
Micropaleontologist
University of Birmingham
50 Brackvede Park
Enniskillen
Co. Fermanagh, BT74 7ND
Northern Ireland
aislingbroderick56@gmail.com

Kevin Brown
Structural Geologist
University of California San Diego
IGPP, Scripps Institute of Oceanography
9500 Gilman Drive MC 0225
La Jolla CA 92093-0225
USA
kmbrown@ucsd.edu

Ana Crespo-Blanc
Structural Geologist
Department of Geodynamics
IACT, Faculty of Sciences
University of Granada
CSIC, C/Fuentenueva s/n
18071 Granada
Spain
acrespo@ugr.es

Emilie Even
Geochemist
Department of Geosciences
Osaka City University
3-3-138 Sugimoto, Sumiyoshi-ku
Osaka 558-8585
Japan
even.e@sci.osaka-cu.ac.jp

Shigeshi Fuchida
Gas Chemistry Specialist
Department of Geoscience
Osaka City University
3-3-138 Sugimoto, Sumiyoshi-ku
Osaka 558-8585
Japan
sfuchida@sci.osaka-cu.ac.jp

Rina Fukuchi
Sedimentologist
Department of Earth and Planetary Science
The University of Tokyo
7-3-1 Hongo, Bunkyo-ku
Tokyo 113-0033
Japan
fukuchi@eps.s.u-tokyo.ac.jp

Sebastian Hammerschmidt
Gas Chemistry Specialist
MARUM-Center for Marine Environmental Sciences
University of Bremen
Leobener Strasse
28359 Bremen
Germany
hammerschmidt@uni-bremen.de

Pierre Henry
Physical Properties Specialist
Centre Européen de Recherche et d'Enseignement des Géosciences de l'Environnement
Aix-Marseille Université
3 Place Victor Hugo
13331 Marseille Cedex 3
France
henry@cerege.fr

Matthew Josh
Physical Properties Specialist
The Commonwealth Scientific and Industrial Research Organization
Earth Science and Resource Engineering
26 Dick Perry Avenue
Kensington WA 6151
Australia
Matthew.josh@csiro.au

María José Jurado
Downhole Logging Specialist
Institute of Earth Sciences Jaume Almera ICTJA
Spanish Research Council CSIC
Lluis Sole Sabaris s/n
E-08028 Barcelona
Spain
mjjurado@ictja.csic.es

Hiroko Kitajima
Physical Properties Specialist
Geological Survey of Japan
National Institute of Advanced Industrial Science and Technology
Central 7, 1-1-1 Higashi
Ibaraki 305-8567
Japan
h-kitajima@aist.go.jp

Manami Kitamura
Physical Properties Specialist
Department of Earth and Planetary Systems Science
Hiroshima University
1-3-1 Kagami-yama,
Higashi Hiroshima, 739-8526
Japan
kitamuram@hiroshima-u.ac.jp

Ana Maia
Sedimentologist
School of Earth and Ocean Sciences
Cardiff University
Main Building, Room 1.59
Park Place
Cardiff CF10 3YE
United Kingdom
MaiaAR@cardiff.ac.uk

Makoto Otsubo
Structural Geologist
Geological Survey of Japan
National Institute of Advanced Industrial Science and Technology
Central 7, 1-1-1 Higashi
Ibaraki 305-8567
Japan
otsubo-m@aist.go.jp

James Sample
Geochemist
School of Earth Sciences and Environmental Sustainability
Geology Program
Northern Arizona University
Flagstaff AZ 86011-4099
USA
James.sample@nau.edu

Anja Schleicher
Sedimentologist
Department of Earth and Environmental Sciences
University of Michigan
1100 North University Avenue
Ann Arbor MI 48109
USA
aschleic@umich.edu

Hiroki Sone
Downhole Logging Specialist
Section 3.2 Geomechanics and Rheology
GFZ German Research Centre for Geosciences
Telegrafenberg
14473 Potsdam
Germany
sone@gfz-potsdam.de

Chen Song
Sedimentologist
Department of Geological Sciences
University of Missouri-Columbia
101 Geology Building
Columbia MO 65211-1380
USA
csrg8@mail.missouri.edu

Robert Valdez
Physical Properties Specialist
The Pennsylvania State University
Department of Geosciences
University Partk PA 16802
USA
rdv116@psu.edu

Yuzuru Yamamoto
Structural Geologist
Institute for Research on Earth Evolution
Japan Agency for Marine-Earth Science and Technology
3173-25 Showa-machi
Kanazawa-ku, Yokohama
Kanagawa 236-0001
Japan
yuzuru-y@jamstec.go.jp

Kiho Yang
Sedimentologist
Department of Earth System Sciences
Yonsei University
237 Science-Hall Sinchon-dong
Seodaemun-gu
Seoul 120-749
Korea
khyang@yonsei.ac.kr

Operation liaison

Kyuichi Kanagawa
Department of Earth Sciences
Chiba University
1-33 Yayoi-cho, Inage-ku
Chiba 263-8522
Japan
kyu_kanagawa@faculty.chiba-u.jp

NanTroSEIZE chief project scientists

Masataka Kinoshita
Chief Project Scientist
Institute for Research on Earth Evolution
Japan Agency for Marine-Earth Science and Technology
2-15 Natsushima-cho, Yokosuka
Kanagawa 237-0061
Japan
masa@jamstec.go.jp

Harold Tobin
Chief Project Scientist
Department of Geology and Geophysics
University of Wisconsin-Madison
1215 West Dayton Street
Madison WI 53706
USA
htobin@wisc.edu

NanTroSEIZE specialty coordinators

Toshiya Kanamatsu
Paleomagnetism/Biostratigraphy
Institute for Research on Earth Evolution
Japan Agency for Marine-Earth Science and Technology
2-15 Natsushima-cho, Yokosuka
Kanagawa 237-0061
Japan
toshiyak@jamstec.go.jp

Gaku Kimura
Structural Geology
Department of Earth and Planetary Science
Graduate School of Science
University of Tokyo
7-3-1 Hongo, Bunkyo-ku
Tokyo 113-0033
Japan
gaku@eps.s.u-tokyo.ac.jp

Gregory Moore
Core-Log-Seismic Integration
Department of Geology and Geophysics
University of Hawaii
1680 East-West Road
Honolulu HI 96822
USA
gmoore@hawaii.edu

Demian Saffer
Physical Properties
The Pennsylvania State University
Deike Building
University Park PA 16802
USA
dsaffer@psu.edu

Michael B. Underwood
Sedimentology
University of Missouri
307 Geology Building
Columbia MO 65211
USA
underwoodm@missouri.edu

Geoff Wheat
Geochemistry
School of Fisheries and Ocean Sciences
University of Alaska Fairbanks
PO Box 475
Moss Landing CA 99775
USA
wheat@mbari.org

Shipboard personnel and technical representatives

Captains (Mantle Quest Japan)
Yukio Dowaki
Yuji Onda
Takemasa Kobayashi

Offshore Installation Managers (Mantle Quest Japan)
Peter Hetherington
Masayuki Kawasaki

Operations Superintendents (CDEX)
Yoshinori Uematsu
Tomokazu Saruhashi
Ikuo Sawada

Drilling Engineers (CDEX)
Daiji Ikenomoto
Sho Kataoka
Satoshi Yamada
Takahiro Yokoyama

Downhole Tools Engineers (Halliburton)
Laurynas Cernauskas
Wedcharat Chuaybudda
Feng Pang
Gustavo Zarif Camacho Davila
Monpanu Galjaru
Joseph Brett Lyman
Alex Munro
Adrianus Andi Prijatno
Cedric Vanva Lutonda

Directional Drilling Engineers (Halliburton)
Bob Manjenic
Daniel Justin Priestly
Gavin Meikle

Mud Logging Engineers (Geoservices)
Myo Kyaw
Maung Ya Wai
Nguyen Luc
Htoo Lin
Danang Adeyaksa
Mohd Alherdi
Salman Al Azzni
Pawan Kuma
Abhigit Duarah
Koh Ming Jen
Liew Shauw Chiu

Mud Engineers (Telnite)
Hiroki Ishikawa
Katsuki Mori
Masato Sawaguchi

Mud Logging Engineers (Geophysical Surveying)
Tsuyoki Fujii
Takumi Kawakami
Kotaro Sayama
Yuki Shimoyama
Hiroshi Ishihara

Wireline Tool Engineers (Schlumberger)
Akira Yoshizawa
Gan Lifeng
Kengo Tsuchida
Yusuke Yoshii

Laboratory Officers (Marine Works Japan)
Satoshi Hirano
Hiroaki Muraki
Tomoyuki Tanaka

Curators (Marine Works Japan)
Yohei Arakawa
Shigako Nigi
Toshikuni Yabuki
Masaru Yasunaga

Laboratory Technicians (Marine Works Japan)
Nobuhiro Anraku
Natsumi Arakawa
Emi Deguchi
Masanori Enoki
Akihiko Fujihara
Toru Fujiki
Yuji Fuwa
Kazuki Harumoto
Takehiro Higashi
Yuya Hitomi
Hiroshi Hoshino
Yuta Iibuchi
Tatsuya Kawai
Daiki Kawata
Yoshiki Kido
Waka Komatsu
Misato Kuwahara
Keitaro Matsumoto

Laboratory Technicians (Marine Works Japan) (continued)
Yoshitomo Mochizuki
Soichi Moriya
Masahiro Nishimura
Atsushi Ohashi
Katsunori Sagishima
Masumi Sakaguchi
Ritsuko Sawada
Hiroyoshi Shimizu
Hiromichi Soejima
Takahiro Suzuki
Kazuma Takahashi
Tomoyuki Takamori
Tatsuya Tanaka
Mika Yamaguchi
Nagisa Yamamoto
Sonoka Wakatsuki

Operation Geologists
Kan Aoike (CDEX)
Takamitsu Sugihara (CDEX)
Takanao Yoshii (JGI)
Ryo Yuasa (JAPEX)

Technical Engineers (CDEX)
Nori Kyo
Eigo Miyazaki
Yasuyuki Yamazaki

Coring Specialist (CDEX)
Yuichi Shinmoto

Publications Specialists (Marine Works Japan)
Yoko Okamoto
Mika Saido
Helen Eri Yamasaki Amsler

Tool Pushers/Coring Supervisors (Mantle Quest Japan)
Geoffrey Cook
Teruyuki Koyama
Charles Ronald Paul
Paul Thornton

Underreamer Engineer (NOV)
Glyn Christopher Edwards

Abstract

The Nankai Trough Seismogenic Zone Experiment (NanTroSEIZE) is a multidisciplinary investigation of fault mechanics and seismogenesis along subduction megathrusts through reflection and refraction seismic imaging, direct sampling by drilling, in situ measurements, and long-term monitoring in conjunction with laboratory and numerical modeling studies. The fundamental objectives of NanTroSEIZE include characterizing the nature of fault slip and strain accumulation, fault and wall rock composition, fault architecture, and state variables throughout an active plate boundary system. As part of the NanTroSEIZE program, operations during Integrated Ocean Drilling Program (IODP) Expedition 348 were planned to extend and case riser Hole C0002F, begun during IODP Expedition 326 in 2010 and continued during Expedition 338 in 2012, from 860 to 3600 meters below the seafloor (mbsf).

Riser operations during Expedition 348 were carried out and deepened the hole to 3056 mbsf, including installation and cementing of 13⅜ inch casing to 2008.9 mbsf and 11¾ inch liner to 2922.5 mbsf. Reaching this depth required two sidetracking operations from the original Hole C0002F, resulting in the designation of Holes C0002N and C0002P for the successively deeper sidetracks. During drilling, a full suite of logging-while-drilling (LWD) and measurement-while-drilling (MWD), mud-gas, and cuttings data were collected over the interval from 2162.5 to 3058.5 mbsf in Hole C0002P, and a partial suite was collected in Hole C0002N. The interval from 2163 to 2218 mbsf was cored with the rotary core barrel (RCB). Reentry during planned future riser drilling operations will deepen the hole to penetrate the megasplay fault at ~4600–5000 mbsf.

Additionally, a test hole for a prototype slimhole small-diameter RCB (SD-RCB) coring system, Hole C0002M, was drilled in riserless mode near Hole C0002F. The hole was advanced to 475 mbsf, where four cores were collected to 512.5 mbsf.

Overall, Expedition 348 sampled and logged a deep interval in Holes C0002N and C0002P within the inner accretionary wedge, from 856 to 3056 mbsf, including a never-before sampled zone in the lowermost ~1 km of drilling. Cores were collected over a 55.5 m interval from 2163 to 2218.5 mbsf. The sampled sedimentary rocks are composed of hemipelagic sediment and fine turbidite with rare ash. The entire interval from ~2145.5 to 2945.5 mbsf has a depositional age of 9.56–10.73 Ma based on nannofossil first and last occurrence data, which is consistent with accretion of a middle Miocene section of either lower Shikoku Basin equivalent or Miocene-age trench

fill; facies analysis suggests the former. Bedding attitudes were ubiquitously steep, measured at 60°–90° in both cores and resistivity image logs. A range of structural fabrics was sampled, including common development of scaly clay fabrics with polished and slickensided clayey surfaces at many depths throughout the drilled interval. Structural fabrics became progressively stronger with depth, and carbonate cement and veins became prevalent below 2100 mbsf. In the cored interval, a well-developed foliated fault zone was identified at 2204.9–2205.8 mbsf with unknown overall displacement sense or amount. This zone contains abundant carbonate cement and vein fill. Log data interpretation suggests at least one additional significant fault zone at ~2220 mbsf, based on fracture intensity and bedding dip anomalies, including apparent broad folds and overturned bedding. Log data also show that *P*-wave velocity (V_P) and resistivity follow a trend of increasing with depth to ~1600 mbsf but vary little from this depth to the bottom of the hole. Average V_P actually decreases slightly with depth over this interval, perhaps due to progressively increasing clay content with depth, increased fracturing or rock damage, or pore fluid overpressure.

Introduction

The Integrated Ocean Drilling Program (IODP) Nankai Trough Seismogenic Zone Experiment (NanTroSEIZE) is a multiexpedition, multistage project focused on understanding the mechanics of seismogenesis and rupture propagation along subduction plate boundary faults. The drilling program includes a coordinated effort to sample and instrument the plate boundary system at several locations off-shore the Kii Peninsula (Kinoshita et al., 2009) (Figs. **F1, F2**). The main objectives are to understand

- The mechanisms and processes controlling the updip aseismic–seismic transition of the megathrust fault system,
- The processes of earthquake and tsunami generation,
- The mechanics of strain accumulation and release,
- The absolute mechanical and elastic strength of the plate boundary fault and surrounding upper and lower plate crustal material, and
- The potential role of a major upper plate fault system (termed the "megasplay" fault) in seismogenesis and tsunamigenesis.

Along the Nankai margin, high-resolution seismic reflection profiles across the outer wedge of the accretionary prism clearly document a large out-of-sequence thrust-fault system (the megasplay fault, after Park et al., 2002) (Fig. **F2**) that branches from the

plate boundary décollement close to the updip limit of inferred coseismic rupture in the 1944 Tonankai Mw 8.2 earthquake (Fig. **F1**). Several lines of evidence indicate that the megasplay system is geologically active (Kimura et al., 2011) and may participate in coseismic slip (e.g., Sakaguchi et al., 2011). However, the partitioning of strain between the décollement zone and the megasplay system (Fig. **F2**) and the nature and mechanisms of fault slip as a function of depth and time on the megasplay are not understood. One of the main objectives of the NanTroSEIZE project is to document the role of the megasplay fault in accommodating plate motion (both seismically and interseismically) and to characterize its mechanical and hydrologic behavior.

IODP Expeditions 314, 315, and 316 were carried out as a unified drilling program collectively known as NanTroSEIZE Stage 1 (Tobin et al., 2009a). Eight sites were selected for riserless drilling to target the frontal thrust region, the midslope megasplay fault region, and the Kumano forearc basin (Figs. **F1, F2**). Site C0002 was the preparatory pilot site for planned deeper riser drilling and operations, whereas the other sites primarily targeted fault zones in the shallow, presumed aseismic, portions of the accretionary complex (Kinoshita et al., 2009). Expedition 314 was dedicated to in situ measurement of physical properties and borehole imaging through logging while drilling (LWD) (Tobin et al., 2009b). Expedition 315 was devoted to core sampling and downhole temperature measurements at sites in the megasplay region and in the forearc basin (Ashi et al., 2009). Expedition 316 targeted the frontal thrust and megasplay fault in their shallow, aseismic portions (Screaton et al., 2009).

Stage 2 of NanTroSEIZE comprised four IODP expeditions (319, 322, 332, and 333), with the aims of building on the results of Stage 1, characterizing the subduction inputs from the Philippine Sea plate, and preparing for later observatory installations for long-term monitoring of deformation at the updip limit of the seismogenic zone (Expedition 319 Scientists, 2010; Underwood et al., 2010; Expedition 332 Scientists, 2011; Expedition 333 Scientists, 2012).

NanTroSEIZE Stage 3 started with IODP Expedition 326, during which a 20 inch casing string was installed in Hole C0002F to 860 mbsf (Expedition 326 Scientists, 2011) and continued with Expedition 338 (Strasser et al., 2014a), during which it was originally planned to deepen Hole C0002F to 3600 mbsf. However, operations had to be aborted because of mechanical and weather-related events after drilling to ~2010 mbsf. Additional casing was not installed during Expedition 338, and Hole C0002F was suspended with drilling mud left in the open hole below the 20 inch casing shoe at 874 mbsf. The original objective of Expedition 338 was to investigate the proper-

ties, structure, and state of stress within the hanging wall above the locked plate boundary at Site C0002 and advance the hole for further deepening during a later expedition, and these remained the primary goals of Expedition 348. During Expedition 348, the hole was sidetracked below the 20 inch casing shoe, and the interval to 2300 mbsf (renamed Hole C0002N) was drilled with measurement while drilling (MWD) and cased, and then sidetracked again (producing Hole C0002P) and drilled with limited coring and LWD/MWD to 3056 mbsf, with 11¾ inch liner emplaced to 2922.5 mbsf.

Site C0002 is the centerpiece of the NanTroSEIZE project, as it is planned to access the plate interface fault system at a location where it is believed the fault system to be capable of seismogenic locking and slip and to have slipped coseismically in the 1944 Tonankai earthquake (e.g., Ichinose et al., 2003). This zone also coincides with the location of repeated clusters of very low frequency earthquakes (VLFE) (Ito and Obara, 2006; Sugioka et al., 2012) and of the first tectonic tremor recorded in an accretionary prism setting (Obana and Kodaira, 2009). To access, sample, and monitor these deeper zones, Hole C0002F was deepened, with the ultimate goal of penetrating the megasplay fault and for the future installation of a long-term observatory (Fig. **F3**).

Background and objectives

Geological setting

Nankai Trough is formed by subduction of the Philippine Sea plate to the northwest beneath the Eurasian plate at a rate of ~4.1–6.5 cm/y (Fig. **F1**) (Seno et al., 1993; Miyazaki and Heki, 2001). The convergence direction is slightly oblique to the trench, and Shikoku Basin sediment is actively accreting at the deformation front. Nankai Trough has been one of the focus sites for studies of seismogenesis by both IODP and the U.S. MARGINS initiative, based on the wealth of geological and geophysical data available. A better understanding of seismic and tsunami behavior at margins such as Nankai is relevant to assessment of hazard to heavily populated coastal areas.

Subduction zones like the Nankai Trough, where most great earthquakes (Mw > 8.0) occur, are especially favorable for study because the entire downdip width of the seismogenic zone ruptures in each event, suggesting that the zone of coseismic rupture in future large earthquakes may be more predictable than for smaller earthquakes. The Nankai Trough region has a 1300 y historical record of recurring great earthquakes that are typically tsunamigenic, including the 1944 Tonankai Mw 8.2 and

1946 Nankai Mw 8.3 earthquakes (Fig. **F1**) (Ando, 1975; Hori et al., 2004). The rupture area and zone of tsunami generation for the 1944 event are now reasonably well understood (Ichinose et al., 2003; Baba et al., 2005). Land-based geodetic studies suggest that currently the plate boundary thrust is strongly locked (Miyazaki and Heki, 2001). Similarly, the relatively low level of microseismicity near the updip limits of the 1940s earthquakes (Obana et al., 2001) implies significant interseismic strain accumulation on the megathrust. However, recent observations of VLFE within or just below the accretionary prism in the drilling area (Obara and Ito, 2005; Sugioka et al., 2012) demonstrate that strain release along the megathrust is not restricted to slow interseismic strain accumulation punctuated by recurring great earthquakes. Slow slip phenomena, including episodic slow slip events and nonvolcanic tremor (e.g., Schwartz and Rokosky, 2007), are also known to occur near the downdip edge of the great earthquake rupture zone (Ito et al., 2007). In the subducting Philippine Sea plate below the rupture zone, weak seismicity is observed (Obana et al., 2005). Seaward of the subduction zone, deformation of the incoming oceanic crust is suggested by microearthquakes as documented by ocean-bottom seismometer (OBS) studies (Obana et al., 2005).

The region offshore the Kii Peninsula on Honshu Island was selected for seismogenic zone drilling for several reasons. First, the rupture area of the 1944 Mw 8.2 Tonankai event is well constrained by recent seismic and tsunami waveform inversions (e.g., Tanioka and Satake, 2001; Kikuchi et al., 2003). Slip inversion studies suggest that only in this region did past coseismic rupture clearly extend shallow enough for drilling (Ichinose et al., 2003; Baba and Cummins, 2005), and an updip zone of large slip has been identified and targeted. Notably, coseismic slip during events like the 1944 Tonankai earthquake may have occurred on the megasplay fault in addition to the plate boundary décollement (Ichinose et al., 2003; Baba et al., 2006; Sakaguchi et al., 2011). The megasplay fault is therefore a primary drilling target equal in importance to the basal décollement. Second, OBS campaigns and onshore high-resolution geodetic studies (though of short duration) indicate significant interseismic strain accumulation (e.g., Miyazaki and Heki, 2001; Obana et al., 2001). Finally, the drilling targets are within the operational limits of riser drilling by the D/V *Chikyu* (i.e., maximum of 2500 m water depth and 7000 m subseafloor penetration). In the seaward portions of the Kumano Basin, the seismogenic zone lies <6000 m beneath the seafloor (Nakanishi et al., 2002).

Seismic studies and site survey data

A significant volume of site survey data has been collected in the drilling area over many years, including multiple generations of 2-D seismic reflection (e.g., Park et al., 2002), wide-angle refraction (Nakanishi et al., 2002), passive seismicity (e.g., Obana et al., 2001, 2005), heat flow (Yamano et al., 2003), side-scan sonar, swath bathymetry, and submersible and remotely operated vehicle (ROV) dive studies (Ashi et al., 2002). In 2006, Japan and the United States conducted a joint 3-D seismic reflection survey over an ~11 km × 55 km area, acquired by Petroleum GeoServices (Moore et al., 2009). This 3-D data volume is the first deep-penetration, fully 3-D marine survey ever acquired for basic research purposes and has been used to

1. Refine selection of drill sites and targets in the complex megasplay fault region,
2. Define the 3-D regional structure and seismic stratigraphy,
3. Analyze physical properties of the subsurface through seismic attribute studies, and
4. Assess drilling safety (Moore et al., 2007, 2009).

These high-resolution 3-D data are being used in conjunction with petrophysical and geophysical data obtained from core analyses and both wireline logging and LWD to allow extensive and high-resolution integration of core, logs, and seismic data (e.g., Bangs et al., 2009; Kitajima and Saffer, 2012).

Site C0002 summary

Scientific objectives

The primary drilling plan for Expedition 348 was to extend the riser hole at Site C0002 from 860 mbsf to a target depth between 3600 and 4400 mbsf. Because of the unknown condition of the open hole below 860 mbsf left after Expedition 338, a plan was made to sidetrack below the 20 inch casing shoe at 860.3 mbsf and redrill the interval parallel to, but 10–20 m laterally away from, Hole C0002F and then set 13⅜ inch casing and 11¾ inch liner successively.

From previous drilling (Fig. **F4**), we already knew that the Kumano forearc basin sedimentary package comprises the 0–940 mbsf interval and is underlain by deformed sediment of the inner accretionary wedge (e.g., Ashi et al., 2009). The seismic reflection character of the entire zone from ~940 mbsf to the megasplay reflector at ~5200

mbsf exhibits few coherent seismic reflections that would indicate intact stratal packages, in contrast to the outer accretionary wedge seaward of the Kumano Basin region (Figs. **F2, F3;** see also Moore et al., 2009). This seismic character was thought to indicate complex deformation within the inner wedge, perhaps best characterized as a subduction mélange or protomélange.

The main research objectives for this interval were to drill and sample the interior of the accretionary complex in the midslope region beneath the Kumano forearc basin with collection of cores, drill cuttings, and mud gas; collect an extensive suite of LWD logs to characterize the formation; and utilize leak-off test and downhole pressure and mud-weight data to constrain in situ stress state. Sampling and recording downhole data from this previously unsampled interval was driven by the following specific questions:

1. What is the thermal, diagenetic, and metamorphic history of the sedimentary rock below the Kumano Basin?
2. What is the dehydration budget for hydrous minerals (e.g., smectite group clays) and the extent of dehydration reaction progress as a function of depth?
3. What is the mechanical and structural evolution of the inner wedge?
4. Are there indicators of zones of low effective stress and/or high pore fluid pressure?
5. How do the properties of the inner wedge sediments compare with the Shikoku Basin and trench sediments that are input to the wedge?
6. What are the horizontal stress orientations and magnitude within the deep interior of the inner wedge? How does the stress orientation relate to the current state of the earthquake cycle?
7. What is the mechanical state and behavior of the formation and how does it relate to the current state of the upper plate above the seismogenic plate boundary thrust?
8. What are the dominant faulting processes and deformation mechanisms, and how do they vary with depth?

Planned operational strategy

The interval from 856 mbsf to the target depth of 3600 mbsf (or as deep as 4400 mbsf, depending on drilling conditions and available time) was to be drilled in riser mode with collection of continuous LWD resistivity, sonic, gamma ray, and annular fluid

pressure logs. During riser drilling, mud return would allow for a comprehensive analysis of drill cuttings and mud gas, as was performed at Site C0009 and Hole C0002F and described by Expedition 319 Scientists (2010) and Moore et al. (2013), respectively. Coring (100 m total) was also planned to sample the inner wedge but was restricted to one interval from 2300 to 2400 mbsf, just below the intended 13⅜ inch casing shoe. After installing the 13⅜ inch casing string to 2400 mbsf, planned operations were to conduct a leak-off test (LOT) and then drill to 3600 mbsf or more and install 11¾ inch liner to that depth. At the end of Expedition 348, the borehole was to be suspended for reentry and further deepening to the planned plate boundary target during a later riser drilling season.

Additionally, as a test of the in-development small-diameter rotary core barrel (SD-RCB) system, a separate riserless hole (C0002M) was to be spudded and drilled to 475 mbsf and cored to 512.5 mbsf (see **"Operations summary";** Tables **T1, T2**). These cores were planned as an engineering test and to compare the core quality to standard RCB cores previously cut from the same interval in Hole C0002B (Ashi et al., 2009); they were to be described and subjected to standard shipboard analysis by the Expedition 348 Scientific Party.

Actual operational results

During Expedition 348, this plan was carried out with overall success, overcoming numerous borehole stability challenges along the way. Hole C0002N was successfully sidetracked from Hole C0002F at 856 mbsf and drilled and cased with 13⅜ inch casing to 2009 mbsf, short of the original 2300 mbsf objective. A stuck and severed bottom-hole assembly (BHA) in the 13⅜ inch casing shoe (see **"Operations summary"**) necessitated a second sidetrack operation, this time through casing, which was successful. The borehole was then extended to 3058.5 mbsf, including a coring interval of 60 m (reduced from 100 m because of time pressure) and cased with the 11¾ inch liner to a final casing depth of 2922.5 mbsf, some 677.5 m shallower than the originally planned target. A full suite of LWD logs were collected, as well as cuttings at 5 m intervals and a 55.5 m coring interval with overall recovery of 56.7%.

Scientific results

Lithology

During Expedition 348, four lithologic units were identified at Site C0002 based on geological and geochemical characteristics of core and cuttings samples (Fig. F5):

- Unit II (475–512.5 mbsf in Hole C0002M),
- Unit III (875.5–975.5 mbsf in Hole C0002N),
- Unit IV (975.5–1665.5 mbsf in Hole C0002N), and
- Unit V (1665.5–2325.5 mbsf in Hole C0002N and 1965.5–3058.5 mbsf in Hole C0002P).

Lithologic Unit II is only described in core from Hole C0002M and is dominated by fine-grained turbiditic deposits. Silty claystone is the main lithology, with subordinate fine-grained sandstone and sandy siltstone. Similar to the equivalent interval (also designated Unit II) in nearby Holes C0002B, C0002K, and C0002L, this unit is composed of lower Kumano forearc basin sediment and is dominated by the hemipelagic mud of distal turbidites (Expedition 315 Scientists, 2009).

Lithologic Unit III, sampled in Hole C0002N (previously sampled in Holes C0002B, C0002D, and C0002F) (Figs. F5, F6A) is dominated by silty claystone with trace amounts of very fine, loose sand containing common glauconite grains. Like Unit II, this unit is also composed of lower Kumano forearc basin sediment.

Lithologic Unit IV, sampled only in Hole C0002N, is dominated by silty claystone, with sandstone as a minor lithology. Sandstone cuttings in this unit are generally very weakly consolidated and occur as disaggregated loose sand. Lithologic Unit IV is divided into five subunits based on sand content (Fig. F6A). Lithologic Unit IV is interpreted as the upper accretionary prism sediment.

Lithologic Unit V was sampled in both Holes C0002N and C0002P (Fig. F6A, F6B, F6C) and is dominated by silty claystone. Fine-grained and moderately cemented sandstone is rarely observed. In Hole C0002P, visual estimates of clay content in the silty claystone increase throughout Subunit VA, and the sediment has a finer texture than material sampled nearby in Hole C0002N. The boundary between Subunits VA and VB (2625.5 mbsf) is defined by a fining of grain size and is located at a depth where the dominant lithology changes from silty claystone to fine silty claystone.

This unit is interpreted as accreted Shikoku Basin hemipelagic deposits or trench fill sediment of the middle Miocene age trench.

Structural geology

Several key observations were made on cuttings in Holes C0002N and C0002P, along with structural analyses of the limited cores retrieved in Hole C0002P. Structures observed in intact cuttings (Fig. **F7**) include slickenlined surfaces, scaly fabric, deformation bands, minor faults, and mineral veins. Slickenlines are observed throughout the entire drilled interval, but scaly fabric is increasingly observed below ~2200 mbsf. The other types of structures are scattered throughout the section.

The limited cored interval exhibits steep bedding dips (Fig. **F7**) ranging from ~45° to 90°, consistent with the observation of steep bedding in borehole resistivity image log data (see **"Logging"**), throughout the interval from 2100–3000 mbsf. A fault zone, 90 cm thick with 2 mm angular clasts, is present in one of the cores (2204.9–2205.8 mbsf; Fig. **F8**). In its present position, the brittle fault zone is associated with a normal faulting sense based on kinematic indicators; however, given the very steep bedding dip documented in cores and throughout the hole in log images, it is plausible that this represents an early thrust rotated after its development or a late normal fault developed in or near its present orientation.

The overall character of the deformation throughout the drilled interval (independent particulate flow with limited evidence for cataclastic deformation) suggests that deformation occurred in a relatively shallow environment (~0–4 km in burial depth), consistent with the present-day depth of this interval in the inner wedge but not precluding modest structural exhumation.

Scanning electron microscope (SEM) images from the upper part of Hole C0002N show little evidence for opal diagenesis, implying maximum temperature (T) <60°–80°C at 1225.5 mbsf (Fig. **F9A, F9B**). In Hole C0002N, the fabric lacks a strongly preferred orientation in clay-rich materials, except along striated microfaults formed by clays (Fig. **F9C, F9D**). These zones are extremely localized, with a thickness of a few micrometers or less. In Hole C0002P below 2200 msbf, SEM images show development of a regularly spaced fabric in sandstones constituted by thin (<0.1–1 µm) clay-dominated shear planes. Toward the base of the hole, below 2625 mbsf, compaction fabrics in clay-rich materials can be observed (Fig. **F9E, F9F**). Observation shows that this fabric is cut by very thin shear zones with almost no wall damage zone.

Biostratigraphy

Preliminary biostratigraphy for Holes C0002M, C0002N, and C0002P is based exclusively on the examination of calcareous nannofossils (Fig. **F10**). There is a general pattern of well- to moderately preserved nannofossils in the upper part of the site (475.09–985.50 mbsf) and moderate to poor preservation below 985.50 mbsf. Assemblages recovered from 475.09–506.68 mbsf (Hole C0002M) are Pleistocene in age, whereas between 875.50 and 3055.50 mbsf (Holes C0002N and C0002P), assemblages indicate late Pliocene to late Miocene age.

Calcareous nannofossils were examined in 25 core samples from Section 348-C0002M-1R-1, 9 cm, to 4R-3, 86 cm, and 287 cuttings samples (348-C0002N-3-SMW through 327-SMW and 348-C0002P-9-SMW through 300-SMW) were examined. A further 25 core samples from Section 348-C0002P-1R-CC, 20 cm, to 6R-CC, 10 cm, were examined.

Hole C0002M

Cores taken from Hole C0002M from 475.00 to 512.50 mbsf yield very well preserved and abundant calcareous nannofossils, indicating a Pleistocene age for the upper part of the section. Assemblages suggest Biozone NN20 and a maximum age of 1.67 Ma based on the last occurrence of *Gephyrocapsa* spp. (<3.92 Ma).

Holes C0002N and C0002P

Cuttings and core samples from Holes C0002N and C0002P between 875.50 and 3055.5 mbsf have assemblages ranging from the late Pliocene to late Miocene. Abundance is relatively lower than in Hole C0002M, and assemblages are less well preserved. Assemblages from Holes C0002N and C0002P show an age range of at least 2.06 Ma to a maximum of 10.734 Ma based mainly on the last occurrence and first occurrence, respectively, of *Discoaster brouweri*. Samples analyzed between 2955.5 and 3055.5 mbsf did not yield any calcareous nannofossil zonal marker species; therefore, the deepest section of Holes C0002N and C0002P cannot be dated.

Paleomagnetism

Remanent magnetization of archive-half sections from Hole C0002P were measured at demagnetization levels of 0, 5, 10, 15, and 20 mT peak fields to identify characteristic directions. Demagnetizations of 10–15 mT successfully removed low-coercivity components, and magnetic directions after demagnetizations indicate stable con-

stant directions (Fig. **F11C, F11F**). Declination, inclination, and intensity profiles after demagnetization at 20 mT are shown in Figure **F12.** The declination profile represents widely scattered directions, indicative of "biscuting" of cores during RCB coring operations. The inclination profile reveals that data are dominantly positive in inclination, and the degrees of the positive inclination in each interval are not constant. For example, the calculated mean inclinations using the method proposed by Arason and Levi (2010) are 34.22° for 2172.45–2174.955 mbsf, 61.83° for 2194.005–2196.985 mbsf, and 36.50° for 2210.0–2215.0 mbsf. Some sections exhibit steep negative inclinations, which occur in relatively short intervals. Interestingly, the 2205.195–2205.515 mbsf interval, which shows a clear negative inclination, corresponds to the brittle fault zone (see **"Structural geology"**). This result suggests different timing of magnetization for this interval than that of the intervals above and below.

In order to elucidate the timing of lock-in of these magnetizations, careful evaluation referencing structural analysis (e.g., bedding) results are required during postcruise study.

Geochemistry

Broadly, geochemical data from Holes C0002N and C0002P support possible important clay-water reactions controlling dissolved cation abundances, the presence of secondary carbonate in faulted sediments, an increase of thermogenic methane with increasing depth, and overall dominance of methane in the gas fraction.

Interstitial water analyses

One 20 cm long whole-round sample of was collected from each of the four Hole C0002M cores. Interstitial water samples were obtained with a new 55 mm diameter Manheim squeezer to conduct tests aimed at defining protocols for maximum squeezing pressure to use on future cores (i.e., to avoid possible stress-induced dehydration of smectite group clays as discussed in Fitts and Brown, 1999). Because these cores had been stored in core liner for several weeks, the likelihood of contamination by drilling fluid was very high, and only chlorinities were determined. Step-wise increasing pressures (up to 112 MPa) were applied to assess the effect of squeezing on measured chlorinity, and interstitial water was sampled at several different time intervals. Chlorinity values are higher than those observed at the same depth interval (470.5–500.5 mbsf) during Expedition 338 (average = 377.8 mM), likely due to contamination, but the range in chlorinity was still low (397–419 mM) compared with a seawater value

of 559 mM. Results from the squeezing experiments show freshening of interstitial water when the same sample was squeezed at higher pressure and for a longer time (Fig. **F13**). The mechanism that induces the freshening of interstitial water at high pressure is not yet understood, and later shore-based experiments will be conducted.

Five whole-round samples (10–41.5 cm in length) were collected from Hole C0002P (Cores 348-C0002P-2R through 6R; 2176.28 to 2211.31 mbsf). Perfluorocarbon tracer data indicate that only Section 348-C0002P-2R-3 had appreciable contamination (~5%) by drilling fluid. Samples were processed to obtain pore water using the GRIND method as was used during Expedition 338 (Strasser et al., 2014a). Salinity and chlorinity alternate between high and low values downhole (Fig. **F14**), a pattern that is paralleled by several other major and minor ions, including Br^-, NH_4^+, Na^+, K^+, Mg_2^+, Ca_2^+, Li, Mn, Ba, Sr, and to a lesser extent Rb and Cs. Although the possibility of localized brines in the formation cannot be excluded, it is unlikely that such large fluctuations in concentrations could occur in samples taken only 10 m apart. It is more likely that the variations in concentrations are related to interaction between interstitial water and rock during core retrieval and sample processing with the GRIND method, perhaps related to variations in clay mineralogy among samples. Two sections (348-C0002P-3R-2 and 5R-2) yielded ion concentrations within interstitial water ranges observed at shallower depths in Holes C0002B and C0002J, with chlorinities of 428 and 387 mM, respectively. If correct, the very low values observed in Hole C0002P require substantial freshening relative to typical seawater values (556 mM), and at these depths the only likely potential source is dehydration of clay-bound waters or opaline silica. Further analysis is necessary to evaluate the significance of the GRIND data.

Carbonate, total organic carbon, total nitrogen, and carbon/nitrogen ratios

Carbonates (as $CaCO_3$), total organic carbon (TOC), and total nitrogen (TN) were analyzed on 15 samples from the four cores from Hole C0002M. $CaCO_3$ ranges from 4.26 to 13.67 wt%, and the median (6.24 wt%) is higher than the two values determined in the same interval from Hole C0002L during Expedition 338 (6.1 and 1.4 wt%). TOC is low (0.46–0.82 wt%) and decreases slightly with depth. TOC and TN are similar to those reported from Expedition 338; the low TOC/TN ratio values in Hole C0002M indicate a marine origin for the organic matter.

In Holes C0002N and C0002P, $CaCO_3$, TOC, and TN were determined from the 1–4 and >4 mm cuttings size fractions (Fig. **F15**). Excluding intervals contaminated by artificial cement, $CaCO_3$ varies from 0.46 to 9.6 wt% (median = 3.2 wt%). Carbonate

abundance generally decreases downhole. A prominent maximum is observed around 1920.5 mbsf, where $CaCO_3$ is as high as 7.94 wt%. A broader maximum at 2620.5 mbsf shows $CaCO_3$ values as high as 5.80 wt%. Cuttings from these depth intervals contain fragments of carbonate veins and sediment with veins, suggesting the local increases in carbonate are associated with fault zones. The abundant carbonate observed in the fault zone in Core 348-C0002P-5R, however, was not evident in the cuttings from the same interval, likely because the signal from the thin fault zone was diluted by mixing of cuttings over a ~5–10 m interval. Increases in CaO and MnO observed in the X-ray diffraction (XRD) data at both carbonate maxima are consistent with the observed increase in $CaCO_3$ and possibly the presence of Mn-bearing carbonate.

In Hole C0002M core samples, TOC is low (0.46–0.82 wt%) and decreases slightly with depth. TOC and TN are similar to Expedition 338. The low TOC/TN ratio values indicate a marine origin for the organic matter. In Holes C0002N and C0002P, TOC values range from 0.47 to 2.07 wt% (median = 0.9 wt%) and gradually decrease with depth (Fig. **F15**). TOC values at the bottom of Hole C0002N (2040–2320 mbsf) do not overlap those at the beginning of Hole C0002P, even though data for $CaCO_3$ and TN do match in the overlapping interval. Data from core samples in Hole C0002P are in closer agreement with those of cuttings from Hole C0002P than with cuttings from Hole C0002N. The relatively high TOC/TN ratios (7.58–35.58; median = 17.53) suggest most of the organic matter is of terrestrial origin. In contrast, TOC/TN in Hole C0002M core samples tend toward a marine origin except for two samples from Sections 348-M0002-2R-4 and 6R-4. Thus, the high TOC/TN ratios in cuttings might reflect contamination by drilling fluid.

Headspace gas and mud-gas results

Continuous-drilling mud-gas monitoring took place while drilling Holes C0002N (838–2330 mbsf) and C0002P (1954–3058 mbsf). The drilling mud-gas content was analyzed for alkanes (methane, ethane, propane, etc.) and nonhydrocarbon (^{222}Rn, He, H_2, Xe, N_2, O_2, etc.) gases by GeoServices and by using the scientific drilling mud-gas monitoring system onboard the *Chikyu* (SciGas system). In Hole C0002N, measurements from the SciGas system yielded lower hydrocarbon gas concentrations compared to the data from GeoServices. Before starting Hole C0002P, the SciGas system was improved, leading to relatively higher gas concentrations and better detection of relative changes in the gas composition in that hole. Headspace gas samples from Hole C0002M and C0002P cores were all dominated by methane, which was as high as 7,354 and 23,455 ppm, respectively. Concentrations found in headspace gas

samples were up to 2 orders of magnitude higher than the drilling mud gas samples from the same interval, indicating underestimation of hydrocarbons by the real-time mud-gas monitoring.

Total gas concentrations were dominated by methane, with maximum concentrations of ~8% at around 1305 mbsf (Fig. **F16**). Downhole gas concentrations steadily declined to <0.2% and rose again at ~2184 mbsf. Overall, ethane and propane were only present in minor concentrations, and higher homologs (i.e., *n*-butane, *i*-butane, *n*-pentane, and *i*-pentane) typically remained <0.01%. Starting at 2200 mbsf, ethane and propane steadily increase with depth. Over the same interval, the Bernard parameter ($C_1/[C_2 + C_3]$) showed an overall decline with depth and when combined with the methane carbon isotope ratio, indicates the onset of a thermogenic regime at ~1700 mbsf (Fig. **F16B**). A clear thermogenic signature was reached at ~2325 mbsf.

Nonhydrocarbon gases were dominated by atmospheric components ($N_2 + O_2$ = 98.3%), which is further supported by an overall N_2/Ar ratio <100. Hydrogen was detected at values up to 0.78% at ~3043 mbsf, and ^{222}Rn values typically remained below 450 Bq/m^3.

Physical properties

Shipboard physical property measurements, including moisture and density (MAD), electrical conductivity, *P*-wave velocity, natural gamma radiation, and magnetic susceptibility, were performed on cuttings samples from 870.5 to 3058.5 mbsf and on core samples from 2163 and 2218.5 mbsf.

MAD measurements were conducted on seawater-washed cuttings ("bulk cuttings") in two size fractions, >4 and 1–4 mm, from 870.5 to 3058.5 mbsf and handpicked intact cuttings from the >4 mm size fractions from 1222.5 to 3058.5 mbsf (Fig. **F17**). The bulk cuttings show grain density of 2.68–2.72 g/cm^3, bulk density of 1.9–2.2 g/cm^3, and porosity of 50%–32%. Compared to the values for bulk cuttings, the intact cuttings show almost the same grain density (2.66–2.70 g/cm^3) but higher bulk density (2.05–2.41 g/cm^3) and lower porosity (37%–18%). The grain density agreement suggests that the measurements on both bulk cuttings and intact cuttings are of good quality, and the differences in porosity and density are real, but the values from the bulk cuttings are affected strongly by artifacts of the drilling process. Thus, the bulk density and porosity data on handpicked cuttings are likely to better represent true formation properties. Combined with MAD measurements on handpicked intact cut-

tings and discrete core samples from previous expeditions, porosity generally decreases from ~60% to ~20% from the seafloor to 3000 mbsf at Site C0002 (Fig. **F17**).

Electrical conductivity and *P*-wave velocity of discrete samples, which were prepared from both cuttings and core samples from 1745.5–3058.5 mbsf, range between 0.15 and 0.9 S/m and 1.7 and 4.5 km/s, respectively. The electrical resistivity (a reciprocal of conductivity) on discrete samples is generally higher than the LWD resistivity data, but the overall depth trends are similar. The *P*-wave velocity of discrete samples is lower than the LWD *P*-wave velocity (see **"Logging"**) between 2200 and 2600 mbsf, whereas the two are in closer agreement below 2600 mbsf.

Logging

Log data acquisition

The LWD data included natural gamma ray, electrical resistivity logs, electrical resistivity images, sonic velocity, and sonic caliper logs (Fig. **F18A, F18B**). These data were collected together with MWD data from 859.5 to 2329.3 mbsf (2827.0–4296.8 mBRT [meters below rotary table]) in Hole C0002N and from 2162.5 to 3058.5 mbsf (4130–5026 mBRT) in Hole C0002P. Data from the two runs overlapped between 1962.6 and 2008.5 mbsf (between 3930.2 and 3976 mBRT). In Hole C0002P, LWD data were collected after coring was conducted from 2163 to 2218.5 mbsf (4130.5–4186 mBRT). The cored interval was logged as the borehole was reamed and enlarged from 10⅝ to 12¼ inch diameter, and then the formation below was logged as the borehole was newly drilled.

There were four major occurrences of long exposure times during the drilling of Hole C0002N (1205–1221, 1662–1678, 1992–2008, and 2022–2038 mbsf). Resistivity values at these depth ranges are both noisy and anomalously low. In Hole C0002P, resistivity data in the cored interval show possible signs of minor mud filtrate invasion and/or wellbore failure.

Hole C0002N

Log data characterization and interpretations

Log Units I–III were identified during IODP Expeditions 314 and 332 for Hole C0002A and C0002G (Expedition 314 Scientists, 2009; Expedition 332 Scientists, 2011).

During Expedition 338, Hole C0002F was drilled (Strasser et al., 2014b), and the bottom of Unit III was identified, which was also the first unit drilled during Expedition 348 in Hole C0002N (Fig. **F18A**).

Log Unit III (859.5–915.0 mbsf) (Fig. **F19**) has an average gamma ray value of 61.6 gAPI and shows a general trend of gamma ray increase of ~20 gAPI down to the basal boundary at 915.0 mbsf. There, a drop of ~25 gAPI is interpreted as a change in lithology from clay-dominated sediment at the base of Unit III to sandy hemipelagic sediment at the top of Unit IV.

Gamma ray and resistivity data show the largest variability in log Unit IV, with average gamma ray values of 66.5 gAPI. We defined five subunits based on overall trends in log response and comparison with the subunits defined during Expedition 338 in Hole C0002F. The base of Unit IV shows a sharp change in the average natural radioactivity to higher values.

Log Unit V (1656.3–total depth) is interpreted to be homogeneous and clay rich overall based on the relatively small fluctuation of log responses and the uniformly high gamma ray values, in agreement with the descriptions of core cuttings lithologies (see **"Lithology"**). Three subunits were defined in Unit V based on variations in log responses that reflect the amount of silt and (occasionally) sand. Gamma ray values average around 86 gAPI throughout Unit V, with variations of up to 28 gAPI. The log Unit IV/V boundary at 1656.3 mbsf is marked by a shift of ~20 gAPI in the gamma ray data and a local spike in resistivity.

Correlation with previous Site C0002 LWD data

We correlated LWD data from Hole C0002F with Hole C0002N, with a vertical offset (depth shift) of ~16 m. Different tools were used, however, leading to potential differences in data quality, resolution, and accuracy among logs. The comparison and correlation is based on natural gamma radioactivity and resistivity. Previously existing resistivity images, including bedding and structural interpretation, were only available for Holes C0002A and C0002F. Comparison with preliminary analysis of Hole C0002P images confirms that log Units IV and V are highly deformed. The log Unit III/IV boundary was correlated between Holes C0002A and C0002F (Fig. **F20**). Measurements of bedding in both holes suggest that the boundary between Units III and IV is an unconformity, as reported previously (Moore et al., 2013). Because Unit IV has more variability in log response, due to the complex geology and relatively variable lithology (from predominantly claystone to silt and sand), it was difficult to

match in detail, but overall trends were consistent in all data sets. The top of logging Unit V is a very sharp boundary for both Holes C0002N and C0002F. Both holes are marked by a ~20 gAPI shift in gamma ray values and changes in resistivity response. The boundary is offset by 18.3 m between the two holes. Image logs reveal a heavily deformed section around this boundary, suggesting that the offset may be structurally related.

Hole C0002P

Log data characterization and interpretation

No major or abrupt change was identified in the log data acquired over the Hole C0002P interval; therefore, changes in trends of log response and values are interpreted as relatively minor in terms of lithology. Only subunits, likely caused by tectonic structure rather than lithologic variability, were defined within this interval of logging Unit V.

From the top to the bottom of the section, LWD tools recorded an increasing trend in gamma radiation (75–95 gAPI), with decreasing resistivity followed by an increasing trend toward the bottom of the borehole. Compressional acoustic slowness/velocity shows constant or decreasing velocity from top to bottom. Within shorter intervals, the overall decrease in velocity is the result of discrete steps in velocity (Fig. **F21**). The most prominent drops in velocity can be identified toward the bottom of logging Subunit Ve.

The logging subunit boundaries we define in Hole C0002P are based on the log character and relative values for the same depth intervals and in the absence of significant compositional changes described from cuttings (see **"Lithology"**). We interpreted the background lithology as hemipelagic silty claystone with relatively constant gamma ray values. Variations in the overall trend seen as excursions and spikes in log values were interpreted as permeable sands, cemented sands or veins, and potential ash layers. The depth intervals for logging subunits are shown on Table **T3** together with the average, minimum, and maximum values of gamma radioactivity, resistivity, and acoustic slowness/velocity.

Resistivity images interpretation

Bedding and structures

Bedding orientations could be measured and characterized throughout the logged interval, with gaps in coverage only at strongly deformed zones where bedding planes are not recognizable in the image logs. Bedding dips predominantly steeply to the northwest (varying from 60° to 90°) (Fig. **F22**). Locally, south- to southeast-dipping beds are also noted, especially between 2600 and 2750 mbsf. Due to the severity of dip changes and high density of fractures and faults, we interpret this section as strongly structurally deformed. A decrease in dip angle was observed from 2860 mbsf (very steep, ~90°) to 3040 mbsf (~60°) at the bottom of the logged section.

The overall structure defined by bedding and structure interpretation suggests that the drilled interval intersects several faulted blocks. Fractures and faults are generally steeply dipping with a range of dips between ~30° and 90° and a wide range of orientations. Fracture density varies with depth, with the highest concentration in the lower section of logging Subunit Vd. Numerous faults with minimal throw or microfaults were also observed.

Wellbore failures

The most obvious and prominent wellbore failures were concentrated in the upper 67 m of Hole C0002P, where the borehole experienced a long exposure time from previous drilling and coring (Fig. **F23**). From 2150 to 2163 mbsf, the borehole is nearly washed out, although resistivity images indicate a preferential development of northwest–southeast breakouts. This section was drilled before coring took place and was opened to a greater width during LWD recording. Breakout widths (defined as the full angular width of one breakout of the pair) average 95° and reach a maximum of 140°. In the cored section between 2163 and 2218.5 mbsf, clear continuous breakouts were observed in the same northwest–southeast direction as higher in the hole but with moderate angular widths (average = 70°). Here, a borehole cross-section from sonic caliper data showed enlargement of borehole diameter in an orientation consistent with the breakouts identified in the image log. For the upper cored section (shallower than 2218.5 mbsf), the length-weighted average value of the breakout azimuths is in the N35°W/S35°E direction. This suggests that the direction of the maximum horizontal principal stress (S_{Hmax}) in the upper 68.5 m of the imaged well is in the northeast–southwest direction.

Below 2163 mbsf, the occurrences of wellbore failures were sparse, and their widths are much smaller (average = 23°) compared to the depth ranges above. With the exception of several features identified shallower than 2600 mbsf, it was not possible to conclusively classify these features as breakouts even with the aid of sonic caliper data, although their orientations are consistent with those observed at the cored section of the well. Some narrow wellbore failures observed toward the bottom of the well appear different from the breakouts above and may possibly be drilling-induced tensile fractures.

Preliminary scientific assessment

Because the primary scientific target of the Site C0002 riser drilling is the plate boundary fault zone at depth, the most important objectives of Expedition 348 were a hybrid of (1) technical milestones in the form of achieving a depth and casing target for future deepening and (2) scientific goals of investigating the structure, lithology, physical properties, fluid content, and state of stress in the middle of the inner wedge.

Technical objectives

The highest priority requirement for this expedition was to deepen the hole and set the stage so that the main target reflector at ~4600–5000 mbsf could be reached in future riser drilling. Toward this end, we had a goal to extend the cased borehole from 860 to 3600 mbsf, bypassing the collapsed uncased zone from Expedition 338 drilling of Hole C0002F (2006 mbsf total depth) through a sidetrack below the 20 inch casing shoe (Fig. **F3**), and install 13⅜ inch casing and 11¾ inch liner to reach that intermediate total depth with a stabilized borehole. Despite multiple operational difficulties and, at times, unstable borehole conditions, the 13⅜ inch casing was successfully cemented into place at 2008.9 mbsf, slightly shallower than the planned 2300 mbsf target. A stuck and severed BHA in the 13⅜ inch casing shoe (see **"Operations summary"**) necessitated a second sidetrack operation, this time through casing, which was successful. The borehole was extended to 3058.5 mbsf and cased with the 11¾ inch liner at 2922.5 mbsf, which is 677.5 m shallower than the planned target. Cementing of this liner was a challenge and had to be done with a cement squeeze job, but indications are that the liner was successfully cemented into place.

While it was a disappointment that the full depth objective was not met, it is a substantial achievement that the main borehole was extended and cased more than 2060

m beyond its previous depth. Holes C0002F, C0002N, and C0002P is now the deepest hole ever drilled (and cased) in scientific ocean drilling. With the 11¾ inch shoe shallower than 3000 mbsf depth, a reanalysis of the casing plan to reach total depth will be required (technical review ongoing as of May 2014), but we believe the 5200 mbsf target can still be met in this hole. For these well engineering aspects, the expedition can therefore be deemed a strong partial success.

Scientific objectives

Our goals included characterizing the materials, architecture, and ambient conditions (stress, pore pressure, and chemistry) of the interior of the inner wedge with a suite of LWD logs including images, cuttings analysis, and ~100 m of core samples. In reality, a comprehensive LWD suite was obtained, and high-quality logs were recorded that have yielded a wealth of information on bedding and fracture orientation, seismic velocity, resistivity, gamma radiation, and the novel continuous ultrasonic caliper. These data sets have been (or are being) used to address all planned goals. Cuttings analysis was carried out in greater detail, with refined techniques relative to all previous scientific ocean drilling efforts and has yielded lithologic, structural, and physical properties information at ~10 m vertical spacing resolution. This effort succeeded beyond initial expectations; in particular, the analysis of physical properties such as porosity and *P*-wave velocity on cuttings yielded better than expected results owing to refined techniques used with care by a skilled team. The detailed analysis of structural fabrics in cuttings by optical and SEM methods was also a somewhat unexpected bright spot. Overall, experience has greatly improved the handling of cuttings since Expedition 319, and this aspect was quite successful. In addition, collection of annular pressure-while-drilling data (APWD), LOTs at the upper casing shoe and just below the 13⅜ inch casing sidetrack, and analysis of drilling mud data from riser operations provided additional valuable constraints on in situ stress magnitudes, rock properties, and, with additional analyses, may potentially constrain the in situ pore fluid pressure.

Because of time lost to operational delays, coring was limited to ~60 m and seven cores. More cores would have been preferable to provide material needed for high-priority postexpedition studies of rock properties to best address both scientific and well engineering objectives, but the cores still afforded a wealth of information on the geology of the inner wedge. It was hoped that the cores would yield usable pore water for geochemical analysis; however, the sediment proved to be too strong and low in porosity to yield water. The GRIND method produced some valuable results (see

"Geochemistry") but overall was clearly greatly inferior to direct pore water analysis. This was somewhat disappointing and suggests that the utility and methods of pore water analysis will need to be reevaluated for future deep drilling.

In summary, during Expedition 348, we met our goals of characterizing the deep interior of the inner accretionary wedge in full over the (somewhat reduced) interval that was drilled and sampled. The operational goal of advancing the borehole and leaving it in a stable cased state ready for further deepening also was completed, albeit ~677 m shallower than initially planned.

Operations summary

Transit from Shimizu (port)

Expedition 348 began on 13 September 2013 and ended on 29 January 2014. The *Chikyu* left the port of Shimizu en route for Site C0002. Typhoon Man-yi's approach on 14 September sent the *Chikyu* into waiting on weather (WOW) status; the *Chikyu* remained in WOW status until 16 September and then returned to Site C0002, arriving on 17 September. Upon return to Site C0002, operations began with an ROV dive in Hole C0002F, and then preparation for coring tests with the new coring tool began.

Hole C0002M

Pressure tests of the riser joints were required, so the riser running equipment was rigged down to prepare for testing the SD-RCB assembly. While designated the "small-diameter" coring tool, the SD-RCB core is actually larger than standard RCB cores (7.3 versus 6.6 cm inner diameter); the bit itself has a smaller diameter, 8½ inch versus the standard 10½ inch (or larger) drill bits. The coring BHA (Table T4) was run into the hole on 19 September 2013. Hole C0002M drilling began from 30.5 mbsf (1996.5 mBRT). By 21 September, the BHA had drilled ahead to 475 mbsf, and coring began from that depth (Tables T1, T2), cutting four cores and ending at 512.5 mbsf (final total depth). After coring operations were complete, the BHA was pulled out of hole and recovered to the surface on 22 September.

Hole C0002F

The rig up for riser running began, and the ROV dove to deploy transponders. Pressure tests of riser joints continued until all were secured for another standby at Shion-

omisaki for WOW until 25 September. The *Chikyu* returned to the Site C0002 blowout preventer (BOP) running point, 15 mi northwest of Site C0002 and prepared to run the BOP and riser. From 26 September 2013, the BOP was run down while low-pressure (300 psi) tests of the auxiliary line (kill and choke lines) began. The tests failed and troubleshooting began; it wasn't until 28 September that all the lines passed low- and high- (5000 psi) pressure tests. The BOP, however, was landed on the BOP cart for transit to Mikawa Bay on 29 September to pick up the repaired riser joint. The *Chikyu* returned to the Site C0002 BOP running point once loading was completed. On 1 October, however, the approach of Tropical Storm Fitow returned the *Chikyu* to WOW status until the storm track and an unrelated weather front were observed. The LWD tools were loaded from supply boat during WOW.

Full operations resumed on 5 October; however, two typhoons (Wipha and Francesco) passed by the site, requiring standby and standoff with the disconnected lower marine riser package (LMRP) from the wellhead. Operations resumed on 26 October, when the LMRP was run into the water. The vessel moved to the well center (water depth = 1967.5 mBRT, 1939 m MSL [mud depth below sea level]) and successfully landed and locked the LMRP on the BOP by 31 October. BOP Yellow control pod (POD) pressure tests and Blue POD function tests were conducted on 1 November. The 17 inch LWD and GeoPilot BHA was made up and run in the hole on 2 November, drilling through the two cement plugs. Drilling continued to 850.5 mbsf, when a pressure test of the 20 inch casing was conducted.

Hole C0002N

After circulation for hole cleaning, the sidetrack for Hole C0002N began at 860.3 mbsf on 4 November 2013. Sidetracking continued until the drilling inclination and azimuth reached 5° and 0°, respectively. On 5 November at 1191.5 mbsf, inclination was changed to 0°. There were many occurrences of mud loss, overpull, and WOW while drilling both Holes C0002N and C0002P (Table **T5**). Drilling halted on 9 November (at ~1856 mbsf) when the real-time MWD signal was lost. After several attempts to recover the signal, it was decided to continue drilling without real-time monitoring to 2008.5 mbsf. On 10 November, the LWD BHA was pulled to the rig floor to remove the GeoPilot from the BHA, dump the LWD memory data, replace the MWD pulser, and perform maintenance on the mud pump. The new 17 inch LWD BHA was run into the hole, and drilling resumed from 2008.5 mbsf on 11 November. Target depth was reached at 2330 mbsf on 13 November. On 15 November the LWD BHA was pulled out of the hole, laid down, and LWD memory data was downloaded. Prepara-

tions to run and cement the 13⅜ inch casing began. On 18 November, the casing hanger joint was picked up and the 13⅜ inch casing was run in hole (RIH). Running 13⅜ inch casing continued to 1993.5 mbsf without observing significant drag. Tight spots were encountered while running the casing string, and the casing became stuck at 2024.5 mbsf. Despite all efforts, the casing needed to be pulled back and shortened by 25 casing joints, and a new pressure-assisted drill pipe running tool (PADPRT) assembly was made up on 21 November. Running the shortened 13⅜ inch casing began; no drag larger than 100 kN was observed while running to 1502 mbsf. However, minor mud loss was observed at 1994.5 mbsf. The casing hanger was landed onto the wellhead on 22 November with the 13⅜ inch casing shoe set at 2010 mbsf. The casing was cemented, followed by a 5500 psi pressure test. The BOP Blue POD function and pressure tests were completed by 24 November.

The 12¼ inch drill-out cement BHA was made up, run into the hole, and tagged the top of cement at 1897.7 mbsf on 25 November. After a short halt in operations for WOW, operations resumed with 1.13 specific gravity (sg) drilling mud. Top of cement was tagged, mud was circulated bottoms up, and a casing pressure test began. The pressure test was completed, and preparations for drilling out cement started. On 27 November, drilling confirmed the presence of cement at 2008.5 mbsf, and rig up for the shoe bond test began. The test was successful, and the drill string was pressurized to an equivalent mud weight (EMW) of 1.25 sg for 5 min. Drilling out cement continued, but when drilling reached 2028.4 mbsf, weight on bit (WOB) and the Hydralift Power Swivel (HPS; National Oilwell Varco) torque became unstable, fluctuating and suddenly increasing. The pipe was stuck, and attempts to free the pipe by jarring began, pausing only for derrick inspection. The Schlumberger free point indicator tool (FPIT) was rigged up to test for the exact stuck point in preparation for freeing the drill pipe by controlled explosion. The back-off tool broke the drill pipe at 1886.35 mbsf. The colliding tool was recovered, the drill string was pulled to surface on 30 November, and the back-off point was confirmed and examined. Although seemingly undamaged, the pipe joint was marked and removed from use. Recovery attempts by fishing for the remaining portion of the BHA began from 1 December. After the fish had been jarred 724 times up and 173 times down with no signs of success, the Schlumberger FPIT was rigged up again and confirmed the free pipe point at 1963 mbsf. The colliding tool was run into the hole to 1960.58 mbsf, calibrated the firing depth, and fired. Circulation and bottoms up circulation from 4 December was completed while the Schlumberger wireline tools were rigged down. The collided drill collar was recovered on deck on 5 December, and a quick examination of the drill col-

lar pin end found that its outer diameter had expanded by 9/16 inch (from 8½ to 9 1/16 inches); the pin thread also expanded and cracked.

The decision was made to kick off through the 13⅜ inch casing and begin a new sidetrack to continue drilling. The casing was scraped with a scraper BHA and then pulled out of the hole and laid for Schlumberger cement bond log (CBL) wireline runs to confirm cement levels outside the casing, which is required for the window sidetrack milling. The CBL was run on 7 December and confirmed cement to 1352.5 mbsf. Time was spent with a milling BHA to certify the fish depth (1948 mbsf) before setting a bridge plug and beginning window cutting in the 13⅜ inch casing. Testing with a wireline run found a slight discrepancy (~2 m) in bridge plug depths, so another run with the casing collar locator wireline confirmed the top of plug depth at 1949.5 mbsf. Wireline recovery and rig down was completed early on 9 December.

Between 9 and 11 December, the *Chikyu* performed an emergency disconnect sequence and dismantled the Hydrarack power swivel (HPS) for a magnetic particle (MPI) inspection of the main shaft of the main power unit (MPU). On 11 December, the *Chikyu* returned to the well to land the LMRP and return to milling out with the whipstock BHA. Once it was set at 1945.5 mbsf on 14 December, window milling in the 13⅜ inch casing began.

Hole C0002P

Hole C0002P begins at 1936.5 mbsf, the top of the milling window. Milling out continued to 1954.5 mbsf, stopping to ream and dress the window so that the BHA could freely pass through. After dressing, two LOTs were run (see **"Logging"**). After completion, mud weight was increased to 1.18 sg. The milling BHA was pulled from the hole, and the kick-off BHA was made up and run into the hole on 16 December 2013. The 12¼ inch sidetrack kick-off BHA began alternate rotation and sliding forward to increase inclination and offset from Hole C0002N, while mud weight was raised to 1.23 sg. As with Hole C0002N, several short periods of stuck pipe and WOW occurred during drilling (Table **T5**). Mud weight was raised to 1.28 sg, as the kick-off inclination finally reached 3.9° by 2107.5 mbsf (sensor depth, 16.35 m above the bit) and dropped off by 2162.5 mbsf. After sweeping out the hole, the kick-off BHA was pulled to the rig floor on 21 December. RCB coring operations (Table **T1**) ran from 22 to 24 December (2163.0–2218.5 mbsf; 6 cores; Tables **T2, T4**). The RCB BHA was pulled from the hole and laid down on 25 December. The coring BHA was switched with a new 12¼ inch LWD BHA on 26 December. However, on 27 December, when the bit

reached 2263 mbsf, MWD data telemetry stopped. All troubleshooting attempts failed, so from 28 December it was decided to drill ahead without real-time monitoring. Drilling (with short wiper trips) proceeded to 3058.5 mbsf by 31 December.

Hole C0002P had numerous overpulls and packoffs regularly recurring during drilling to total depth (Table **T5**); each time, the pipe was freed after dropping pumping pressure and working the drill pipe. Reaming out the hole to 3058.5 mbsf was completed by 1 January 2014; a heavy load of cavings continued to arrive at the shale shakers. The HPS stalled three times while working pipe while making connections, and mud weight was increased to 1.32 sg. On 2 January, the LWD BHA was recovered on deck and memory data was downloaded. Gamma ray, APWD, and resistivity data were recovered by 0545 h, and azimuthal sonic (X-BAT) data were recovered by 0615 h, but the azimuthal focused resistivity (AFR) data recovery port was damaged, preventing data download. Data download required shipping the AFR to the Halliburton base in Thailand.

Reaming out the open hole to 14½ inches was performed with the Anderreamer underreamer BHA from 2 January. No logging tools were part of this BHA. The underreamer began reaming open the 12¼ inch hole to 14½ inches from 1963.5 mbsf. Reaming down occasionally paused for mud pump maintenance. Hole opening continued, with nothing more than traces of gas and cavings encountered throughout this period of drilling. From 8 January, several episodes of HPS stalling at 2867.5 mbsf from heave increase were noted. Another cold front weather system required pulling out of the hole for WOW to above the BOP for standby. The cold front passed, and WOW continued until 9 January. On 10 January, reaming up and down encountered frequent HPS stalls, tight spots, and one hole pack-off at 2902.5 mbsf. The pack-off initially had no mud return, but continuously working the pipe and reducing pumping pressure eventually freed the pipe by 1500 h. Backreaming and hole opening operations continued to 12 January, when the Anderreamer underreamer BHA was recovered on deck; the reamer cutters were excessively worn and damaged. A new underreamer BHA was rigged up and run into the hole. Once the BHA reached 1957.5 mbsf the Anderreamer was activated. A series of issues with the mud pumps impacting drilling, with frequent pauses in drilling to swab out and replace cylinders of the mud pumps. Reaming downhole resumed and by 14 January had reached 2960.5 mbsf. Hole opening had progressed 4 m when the hole packed off, leaving the drill pipe stuck in the hole. Operations to free the pipe began immediately, with firing jars, spotting lube, and pulling until the pipe was freed. Sweeping the hole began and circulation and bottoms-up was finished by 15 January. The BHA continued in a series

of wiper trips and reaming, reaching 2964.5 mbsf by 2130 h. Circulation and bottoms-up to clean the hole began and continued until 16 January. It was decided to spot Hi-vis mud (30 m^3) and pull the underreamer to the surface; the BHA was laid down by 1800 h.

With reaming and drilling complete, running and cementing the 11¾ inch liner began. On 18 January, the liner was run to 966.5 m MSL while setting the guide shoe joint, float collar joint, landing collar joint, and the 3½ inch ball in the float collar joint. No drag was observed while running casing. Slack was checked and weight picked up before circulating after breaking pipe to drop the 1¾ inch ball. Setting the liner hanger began; the first three attempts to set the hanger failed. After picking up 1 m and applying pressure, it was confirmed that the hanger had been released. However, it soon became clear that the liner-casing packer had also set when circulation attempts failed. Pressure tests confirmed that the annulus pressure was holding (up to 7.8 MPa), and there was no communication with the formation below. Two LOTs were performed, the second ending in an injection test. The liner packer was pressure tested at 5000 psi for 5 min and then at 4000 psi for 15 min; both tests passed. After the LOTs the liner hanger running tool was pulled to surface, laying out the cement stand on 19 January. The first of two cement "squeezes" was completed early on 20 January. After squeezing, the diverter was pulled from the hole and Hi-vis mud was spotted. The diverter assembly was pulled to surface, and the cement plug was pressure tested on 21 January.

Riser recovery began, and the BOP was disconnected from the wellhead on 22 January, while the ROV set the corrosion cap and recovered transponders. By 23 January, the gooseneck and termination joints had been recovered and riser joints proper began to be recovered; the BOP was recovered and set on the BOP cart by 25 January. The ROV dove to complete transponder recovery. Once complete, the ROV was recovered to the surface, while riser-handling tools were rigged down and general rig equipment services were performed. The *Chikyu* left the site on 29 January for IHI facilities in Irago, Aichi Prefecture (Japan).

References

Ando, M., 1975. Source mechanisms and tectonic significance of historical earthquakes along the Nankai Trough, Japan. *Tectonophysics,* 27(2):119–140. **doi:10.1016/0040-1951(75)90102-X**

Arason, P., and Levi, S., 2010. Maximum likelihood solution for inclination-only data in paleomagnetism. *Geophys. J. Int.,* 182(2):753–771. **doi:10.1111/j.1365-246X.2010.04671.x**

Ashi, J., Kuramoto, S., Morita, S., Tsunogai, U., Goto, S., Kojima, S., Okamoto, T., Ishimura, T., Ijiri, A., Toki, T., Kudo, S., Asai, S., and Utsumi, M., 2002. Structure and cold seep of the Nankai accretionary prism off Kumano—outline of the off Kumano survey during YK01-04 Leg 2 cruise. *JAMSTEC J. Deep-Sea Res.,* 20:1–8. (in Japanese, with abstract in English)

Ashi, J., Lallemant, S., Masago, H., and the Expedition 315 Scientists, 2009. Expedition 315 summary. *In* Kinoshita, M., Tobin, H., Ashi, J., Kimura, G., Lallemant, S., Screaton, E.J., Curewitz, D., Masago, H., Moe, K.T., and the Expedition 314/315/316 Scientists, *Proc. IODP,* 314/315/316: Washington, DC (Integrated Ocean Drilling Program Management International, Inc.). **doi:10.2204/iodp.proc.314315316.121.2009**

Baba, T., and Cummins, P.R., 2005. Contiguous rupture areas of two Nankai Trough earthquakes revealed by high-resolution tsunami waveform inversion. *Geophys. Res. Lett.,* 32(8):L08305. **doi:10.1029/2004GL022320**

Baba, T., Cummins, P.R., and Hori, T., 2005. Compound fault rupture during the 2004 off the Kii Peninsula earthquake (*M* 7.4) inferred from highly resolved coseismic sea-surface deformation. *Earth, Planets Space,* 57(3):167–172. **http://www.terrapub.co.jp/journals/EPS/pdf/2005/5703/57030167.pdf**

Baba, T., Cummins, P.R., Hori, T., and Kaneda, Y., 2006. High precision slip distribution of the 1944 Tonankai earthquake inferred from tsunami waveforms: possible slip on a splay fault. *Tectonophysics,* 426(1–2):119–134. **doi:10.1016/j.tecto.2006.02.015**

Bangs, N.L.B., Moore, G.F., Gulick, S.P.S., Pangborn, E.M., Tobin, H.J., Kuramoto, S., and Taira, A., 2009. Broad, weak regions of the Nankai Megathrust and implications for shallow coseismic slip. *Earth Planet. Sci. Lett.,* 284(1–2):44–49. **doi:10.1016/j.epsl.2009.04.026**

Expedition 314 Scientists, 2009. Expedition 314 Site C0002. *In* Kinoshita, M., Tobin, H., Ashi, J., Kimura, G., Lallemant, S., Screaton, E.J., Curewitz, D., Masago, H., Moe, K.T., and the Expedition 314/315/316 Scientists, *Proc. IODP,* 314/315/316: Washington, DC (Integrated Ocean Drilling Program Management International, Inc.). **doi:10.2204/iodp.proc.314315316.114.2009**

Expedition 315 Scientists, 2009. Expedition 315 Site C0002. *In* Kinoshita, M., Tobin, H., Ashi, J., Kimura, G., Lallemant, S., Screaton, E.J., Curewitz, D., Masago, H., Moe, K.T., and the Expedition 314/315/316 Scientists, *Proc. IODP,* 314/315/316: Washington, DC (Integrated Ocean Drilling Program Management International, Inc.). **doi:10.2204/iodp.proc.314315316.124.2009**

Expedition 319 Scientists, 2010. Expedition 319 summary. *In* Saffer, D., McNeill, L., Byrne, T., Araki, E., Toczko, S., Eguchi, N., Takahashi, K., and the Expedition 319 Scientists, *Proc. IODP,* 319: Tokyo (Integrated Ocean Drilling Program Management International, Inc.). **doi:10.2204/iodp.proc.319.101.2010**

Expedition 326 Scientists, 2011. NanTroSEIZE Stage 3: plate boundary deep riser: top hole engineering. *IODP Prel. Rept.,* 326. **doi:10.2204/iodp.pr.326.2011**

Expedition 332 Scientists, 2011. Site C0010. *In* Kopf, A., Araki, E., Toczko, S., and the Expedition 332 Scientists, *Proc. IODP,* 332: Tokyo (Integrated Ocean Drilling Program Management International, Inc.). **doi:10.2204/iodp.proc.332.103.2011**

Expedition 333 Scientists, 2012. Expedition 333 summary. *In* Henry, P., Kanamatsu, T., Moe, K., and the Expedition 333 Scientists, *Proc. IODP,* 333: Tokyo (Integrated Ocean Drilling Program Management International, Inc.). **doi:10.2204/iodp.proc.333.101.2012**

Fitts, T.G., and Brown, K.M., 1999. Stress-induced smectite dehydration: ramifications for patterns of freshening and fluid expulsion in the N. Barbados accretionary wedge. *Earth Planet. Sci. Lett.,* 172(1–2):179–197. **doi:10.1016/S0012-821X(99)00168-5**

Hori, T., Kato, N., Hirahara, K., Baba, T., and Kaneda, Y., 2004. A numerical simulation of earthquake cycles along the Nankai Trough in southwest Japan: lateral variation in frictional property due to the slab geometry controls the nucleation position. *Earth Planet. Sci. Lett.,* 228(3–4):215–226. **doi:10.1016/j.epsl.2004.09.033**

Ichinose, G.A., Thio, H.K., Somerville, P.G., Sato, T., and Ishii, T., 2003. Rupture process of the 1944 Tonankai earthquake (M_S 8.1) from the inversion of teleseismic and regional seismograms. *J. Geophys. Res.: Solid Earth,* 108(B10):2497. **doi:10.1029/2003JB002393**

Ito, Y., and Obara, K., 2006. Very low frequency earthquakes within accretionary prisms are very low stress-drop earthquakes. *Geophys. Res. Lett.,* 33(9):L09302. **doi:10.1029/2006GL025883**

Ito, Y., Obara, K., Shiomi, K., Sekine, S., and Hirose, H., 2007. Slow earthquakes coincident with episodic tremors and slow slip events. *Science,* 315(5811):503–506. **doi:10.1126/science.1134454**

Kikuchi, M., Nakamura, M., and Yoshikawa, K., 2003. Source rupture processes of the 1944 Tonankai earthquake and the 1945 Mikawa earthquake derived from low-gain seismograms. *Earth, Planets Space,* 55(4):159–172. **http://www.terrapub.co.jp/journals/EPS/pdf/2003/5504/55040159.pdf**

Kimura, G., Moore, G.F., Strasser, M., Screaton, E., Curewitz, D., Streiff, C., and Tobin, H., 2011. Spatial and temporal evolution of the megasplay fault in the Nankai Trough. *Geochem., Geophys., Geosyst.,* 12(3):Q0A008. **doi:10.1029/2010GC003335**

Kinoshita, M., Tobin, H., Ashi, J., Kimura, G., Lallemant, S., Screaton, E.J., Curewitz, D., Masago, H., Moe, K.T., and the Expedition 314/315/316 Scientists, 2009. *Proc. IODP,* 314/315/316: Washington, DC (Integrated Ocean Drilling Program Management International, Inc.). **doi:10.2204/iodp.proc.314315316.2009**

Kitajima, H., and Saffer, D.M., 2012. Elevated pore pressure and anomalously low stress in regions of low frequency earthquakes along the Nankai Trough subduction megathrust. *Geophys. Res. Lett.,* 39(23):L23301. **doi:10.1029/2012GL053793**

Lurcock, P.C., and Wilson, G.S., 2012. PuffinPlot: a versatile, user-friendly program for paleomagnetic analysis. *Geochem., Geophys., Geosyst.,* 13(6):Q06Z45. **doi:10.1029/2012GC004098**

Miyazaki, S., and Heki, K., 2001. Crustal velocity field of southwest Japan: subduction and arc-arc collision. *J. Geophys. Res.: Solid Earth,* 106(B3):4305–4326. **doi:10.1029/2000JB900312**

Moore, G.F., Bangs, N.L., Taira, A., Kuramoto, S., Pangborn, E., and Tobin, H.J., 2007. Three-dimensional splay fault geometry and implications for tsunami generation. *Science,* 318(5853):1128–1131. **doi:10.1126/science.1147195**

Moore, G.F., Park, J.-O., Bangs, N.L., Gulick, S.P., Tobin, H.J., Nakamura, Y., Sato, S., Tsuji, T., Yoro, T., Tanaka, H., Uraki, S., Kido, Y., Sanada, Y., Kuramoto, S., and Taira, A., 2009.

Structural and seismic stratigraphic framework of the NanTroSEIZE Stage 1 transect. *In* Kinoshita, M., Tobin, H., Ashi, J., Kimura, G., Lallemant, S., Screaton, E.J., Curewitz, D., Masago, H., Moe, K.T., and the Expedition 314/315/316 Scientists, *Proc. IODP,* 314/315/316: Washington, DC (Integrated Ocean Drilling Program Management International, Inc.). **doi:10.2204/iodp.proc.314315316.102.2009**

Moore, G., Kanagawa, K., Strasser, M., Dugan, B., Maeda, L., Toczko, S., and the Expedition 338 Scientists, 2013. NanTroSEIZE Stage 3: NanTroSEIZE plate boundary deep riser 2. *IODP Prel. Rept.,* 338. **doi:10.2204/iodp.pr.338.2013**

Nakanishi, A., Takahashi, N., Park, J.-O., Miura, S., Kodaira, S., Kaneda, Y., Hirata, N., Iwasaki, T., and Nakamura, M., 2002. Crustal structure across the coseismic rupture zone of the 1944 Tonankai earthquake, the central Nankai Trough seismogenic zone. *J. Geophys. Res.: Solid Earth,* 107(B1):EPM 2-1–EPM 2-21. **doi:10.1029/2001JB000424**

Obana, K., and Kodaira, S., 2009. Low-frequency tremors associated with reverse faults in a shallow accretionary prism. *Earth Planet. Sci. Lett.,* 287(1–2):168–174. **doi:10.1016/j.epsl.2009.08.005**

Obana, K., Kodaira, S., Mochizuki, K., and Shinohara, M., 2001. Micro-seismicity around the seaward updip limit of the 1946 Nankai earthquake dislocation area. *Geophys. Res. Lett.,* 28(12):2333–2336. **doi:10.1029/2000GL012794**

Obana, K., Kodaira., S., and Yoshiyuki, K., 2005. Seismicity in the incoming/subducting Philippine Sea plate off the Kii Peninsula, central Nankai Trough. *J. Geophys. Res.: Solid Earth,* 110(B11):B11311. **doi:10.1029/2004JB003487**

Obara, K., and Ito, Y., 2005. Very low frequency earthquakes excited by the 2004 off the Kii Peninsula earthquakes: a dynamic deformation process in the large accretionary prism. *Earth, Planets Space,* 57(4):321–326. **http://www.terrapub.co.jp/journals/EPS/pdf/2005/5704/57040321.pdf**

Park, J.-O., Tsuru, T., Kodaira, S., Cummins, P.R., and Kaneda, Y., 2002. Splay fault branching along the Nankai subduction zone. *Science,* 297(5584):1157–1160. **doi:10.1126/science.1074111**

Sakaguchi, A., Chester, F., Curewitz, D., Fabbri, O., Goldsby, D., Kimura, G., Li, C.-F., Masaki, Y., Screaton, E.J., Tsutsumi, A., Ujiie, K., and Yamaguchi, A., 2011. Seismic slip propagation to the updip end of plate boundary subduction interface faults: vitrinite reflectance geothermometry on Integrated Ocean Drilling Program NanTroSEIZE cores. *Geology,* 39(4):395–398. **doi:10.1130/G31642.1**

Schwartz, S.Y., and Rokosky, J.M., 2007. Slow slip events and seismic tremor at circum-Pacific subduction zones. *Rev. Geophys.,* 45(3):RG3004. **doi:10.1029/2006RG000208**

Screaton, E.J., Kimura, G., Curewitz, D., and the Expedition 316 Scientists, 2009. Expedition 316 summary. *In* Kinoshita, M., Tobin, H., Ashi, J., Kimura, G., Lallemant, S., Screaton, E.J., Curewitz, D., Masago, H., Moe, K.T., and the Expedition 314/315/316 Scientists, *Proc. IODP,* 314/315/316: Washington, DC (Integrated Ocean Drilling Program Management International, Inc.). **doi:10.2204/iodp.proc.314315316.131.2009**

Seno, T., Stein, S., and Gripp, A.E., 1993. A model for the motion of the Philippine Sea plate consistent with NUVEL-1 and geological data. *J. Geophys. Res.: Solid Earth,* 98(B10):17941–17948. **doi:10.1029/93JB00782**

Strasser, M., Dugan, B., Kanagawa, K., Moore, G.F., Toczko, S., Maeda, L., and the Expedition 338 Scientists, 2014a. *Proc. IODP,* 338: Yokohama (Integrated Ocean Drilling Program Management International, Inc.). **doi:10.2204/iodp.proc.338.2014**

Strasser, M., Dugan, B., Kanagawa, K., Moore, G.F., Toczko, S., Maeda, L., Kido, Y., Moe, K.T., Sanada, Y., Esteban, L., Fabbri, O., Geersen, J., Hammerschmidt, S., Hayashi, H., Heirman,

K., Hüpers, A., Jurado Rodriguez, M.J., Kameo, K., Kanamatsu, T., Kitajima, H., Masuda, H., Milliken, K., Mishra, R., Motoyama, I., Olcott, K., Oohashi, K., Pickering, K.T., Ramirez, S.G., Rashid, H., Sawyer, D., Schleicher, A., Shan, Y., Skarbek, R., Song, I., Takeshita, T., Toki, T., Tudge, J., Webb, S., Wilson, D.J., Wu, H.-Y., and Yamaguchi, A., 2014b. Site C0002. *In* Strasser, M., Dugan, B., Kanagawa, K., Moore, G.F., Toczko, S., Maeda, L., and the Expedition 338 Scientists, *Proc. IODP,* 338: Yokohama (Integrated Ocean Drilling Program). **doi:10.2204/iodp.proc.338.103.2014**

Sugioka, H., Okamoto, T., Nakamura, T., Ishihara, Y., Ito, A., Obana, K., Kinoshita, M., Nakahigashi, K., Shinohara, M., and Fukao, Y., 2012. Tsunamigenic potential of the shallow subduction plate boundary inferred from slow seismic slip. *Nat. Geosci.,* 5(6):414–418. **doi:10.1038/ngeo1466**

Tanioka, Y., and Satake, K., 2001. Detailed coseismic slip distribution of the 1944 Tonankai earthquake estimated from tsunami waveforms. *Geophys. Res. Lett.,* 28(6):1075–1078. **doi:10.1029/2000GL012284**

Tobin, H., Kinoshita, M., Ashi, J., Lallemant, S., Kimura, G., Screaton, E.J., Moe, K.T., Masago, H., Curewitz, D., and the Expedition 314/315/316 Scientists, 2009a. NanTroSEIZE Stage 1 expeditions: introduction and synthesis of key results. *In* Kinoshita, M., Tobin, H., Ashi, J., Kimura, G., Lallemant, S., Screaton, E.J., Curewitz, D., Masago, H., Moe, K.T., and the Expedition 314/315/316 Scientists, *Proc. IODP,* 314/315/316: Washington, DC (Integrated Ocean Drilling Program Management International, Inc.). **doi:10.2204/iodp.proc.314315316.101.2009**

Tobin, H., Kinoshita, M., Moe, K.T., and the Expedition 314 Scientists, 2009b. Expedition 314 summary. *In* Kinoshita, M., Tobin, H., Ashi, J., Kimura, G., Lallemant, S., Screaton, E.J., Curewitz, D., Masago, H., Moe, K.T., and the Expedition 314/315/316 Scientists, *Proc. IODP,* 314/315/316: Washington, DC (Integrated Ocean Drilling Program Management International, Inc.). **doi:10.2204/iodp.proc.314315316.111.2009**

Underwood, M.B., Saito, S., Kubo, Y., and the Expedition 322 Scientists, 2010. Expedition 322 summary. *In* Saito, S., Underwood, M.B., Kubo, Y., and the Expedition 322 Scientists, *Proc. IODP,* 322: Tokyo (Integrated Ocean Drilling Program Management International, Inc.). **doi:10.2204/iodp.proc.322.101.2010**

Yamano, M., Kinoshita, M., Goto, S., and Matsubayashi, O., 2003. Extremely high heat flow anomaly in the middle part of the Nankai Trough. *Phys. Chem. Earth,* 28(9–11):487–497. **doi:10.1016/S1474-7065(03)00068-8**

Table T1. Drilling summary, Expedition 348.

Hole	Latitude	Longitude	Water depth (mbsl)	Cores (*N*)	Interval cored	Core recovered	Recovery (%)	Drilled interval (m)	Total penetration (m)	Time on site (days)
C0002M	33°18.0058′N	136°38.2397′E	1937.50	4	37.5	16.43	43.8	475–512.5	512.5	1
C0002N	33°18.0507′N	136°38.2029′E	1939.00	0	LWD/MWD	—	—	859.5–2329.3	2320.5	
C0002P	33°18.0507′N	136°38.202′E	1939.00	6	55.5	31.5	56.7	2163–2218.5	2218.5	
	33°18.0507′N	136°38.2029′E	1939.00	0	LWD/MWD	—	—	2163–3058.5	3058.5	
			Total:	10	93	47.93	50.3		8110.0	

LWD = logging while drilling, MWD = measurement while drilling. — = not applicable.

Table T2. Summary of all coring completed during Expedition 348.

Hole	Longitude	Latitude	Water depth (mbsl)	Core	Date/Time on deck (2013; h UTC)	Depth (mbsf)	Advanced (m)	Recovered (m)	Recovery (%)	Drilled interval (mbsf)	Cored interval (m)	Core recovered (m)	Recovery (%)
C0002M	33°18.0058′N	136°38.2397′E	1937.5	1R	21 Sep; 1135	475.0	9.5	5.3	56.0	475–512.5	37.5	16.4	43.8
				2R	21 Sep; 1442	484.5	9.5	4.0	44.2				
				3R	21 Sep; 1726	493.5	9.0	2.5	26.7				
				4R	21 Sep; 1953	503.0	9.5	4.6	48.4				
C0002P	33°18.0507′N	136°38.2029′E	1939.0	1R	23 Dec; 0513	2163.0	9.5	0.4	4.2	2163–2218.5	55.5	31.5	56.7
				2R	23 Dec; 1138	2172.5	9.5	6.1	63.7				
				3R	23 Dec; 1842	2182.0	9.5	2.9	30.3				
				4R	24 Dec; 0353	2191.5	9.5	8.2	86.2				
				5R	24 Dec; 1214	2201.0	8.0	5.5	68.8				
				6R	24 Dec; 2015	2209.0	9.5	8.5	89.1				

Table T3. Log units, Hole C0002P.

Log unit	Depth (mbsf)	Log subunit	Depth (mbsf)	Gamma ray (gAPI)			Acoustic *P*-wave (µs/ft)			RH48PC resistivity (Ωm)		
				Low	High	Mean	Low	High	Mean	Low	High	Mean
V	2163–TD	Vc′	2163–2365.6	58	94	84	83.7	109.8	94.3	1.4	3.6	2.5
		Vd	2365.6–2753	69	102	87	84.4	104.1	92.9	1.4	4.6	2.2
		Ve	2753–3058.5	81	104	95	79.7	106.2	94.2	1.9	4.0	2.6

TD = target depth.

Table T4. Bottom-hole assemblies (BHAs) used during Expedition 348.

Hole	Drilling type	Water depth (mbsl)	Top hole depth (mbsf)	Top hole depth (mBRT)	TD (mbsf)	TD (mBRT)	Bit size (inch)	BHA
C000M	SD-RCB	1937.5	0.0	1967.5	512.5	2480.0	8-1/2	Bit × near-bit sub (w/float and inner tube stabilizer) × DC sub (w/landing ring) × landing sub × head sub (w/ latch sleeve) × 7 inch coring DC (11) × XO × 5.68 inch HWDP (12) × XO × 5 inch DP S-140 (21 stands) × 5-1/2 inch DP S-140 (21 stands) × XO × 5-1/2 inch DP S-150
C000F	LWD/MWD	1939.0	0.0	1967.5	2005.5	3973.0	12-1/4	Bit × GVR × ARC8 × TeleScope × 12-1/8 inch ILS × sonicVISION × 12-1/8 inch stab × 8-1/2 inch DC (1) × CST × Anderreamer × F/S × 9-1/2 inch DC (2) × 17 inch stab × 9-1/2 inch DC (1) × XO × 8-1/2 inch DC (3) × 7-3/4 inch Jar × 8-1/2 inch DC (3) × XO × 5.68 inch HWDP (12) × XO × 5 inch DP S-140 (46 stands) × 5-1/2 inch DP S-150
C000N	Sidetrack	1939.0	860.0	2827.5	2330.0	4297.5	17	Bit × sleeve stab × Geopilot9600 w/near-bit stab × flex collar × 16-7/8 inch ILS × 8 inch DGR × 8 inch EWR × 8 inch PWD × 8 inch HCIM × HOC × MWD down screen × float sub (w/float) × 8-1/2 inch DC (12) × 8 inch hydraulic Jar × 8-1/2 inch DC (2) × XO × 5.68 inch HWDP (12) × XO × 5 inch DP S-140 (53 stands) × XO × 5-1/2 inch DP S-150
C000N	Casing run	1939.0	NA	NA	2009.0	3976.5	NA	13-3/8 inch casing PADPRT × XO × 5-1/2 inch DP S-150 (6 m) × XO × XO × 5-7/8 inch DP NK-155 (3) × 5-7/8 inch DP NK-155 (18 stands) × XO × 6-5/8 inch DP UD-165 (1 stand) × 6-5/8 inch DP (6 m) × 6-5/8 inch DP (31 stands) × CMT stand
C000N	Fishing	1939.0	NA	NA	1886.4	3853.9	NA	Screw-in sub (5¾ inch DSTJ pin) × XO × 5.68 inch HWDP (2) × XO × drilling jar × 8-1/2 inch DC (2) × XO × 5.68 inch HWDP (12) × 5-1/2 inch DP S-150 (21 stands) × XO × XO × 5-7/8 inch DP NK-155 (19 stands) × XO × 6-5/8 inch DP Z-140 (25 stands) × XO × 6-5/8 inch DP UD-165
C000N	WBRRT	1939.0	NA	NA	NA	NA	NA	Jetting sub × XO × 5-1/2 inch DP S-140 (1stand) × XO × 8-1/2 inch DC (1) × 12-1/4 inch stab × 8-1/2 inch DC (5) × XO × 5-1/2 inch DP S-140 (1 stand) × XO × WBRRT × XO × 5-1/2 inch DP pup (6 m) × 5 inch DP S-140 (44 stands) × 6-5/8 inch DP Z-140
C000P	Window milling	1939.0	1935.5	3903.0	1954.5	3922.0	12-1/4	Lead mill × 8-1/2 inch DC (1) × 12-1/4 inch stab × secondary mill × flex mandrel × steering mill × 8-1/2 inch DC (9) × XO × 8-1/2 inch coring DC (12) × XO × 5.68 inch HWDP (12) × XO × 5 inch DP S-140 (26 stands) × 5-1/2 inch DP S-140 (21 stands) × XO × 5-1/2 inch DP S-150 (25 stands) × XO × 6-5/8 inch DP Z-140
C000P	Kick-off	1939.0	1936.5	3904.0	2162.5	4130.0	12-1/4	Bit × motor × 12 inch stab × HOC × DH screen × float sub (w/float) × 8-1/2 inch DC (12) × drilling jar × 8-1/2 inch DC (2) × XO × 5.68 inch HWDP (12) × XO × 5 inch DP S-140 (44 stands) × 5-1/2 inch DP S-140 (21 stands) × XO × 5-1/2 inch DP S-150 (25 stands) × XO × 6-5/8 inch DP Z-140
C000P	RCB	1939.0	2162.5	4130.0	2118.0	4085.5	10-5/8	Bit × bit sub w/stab × RCB core barrel × top sub × head sub × 10-5/8 inch stab × 8-1/2- inch coring DC (12) × coring jar × 8-1/2 inch coring DC (3) × XO × 5.68 inch HWDP(12) × XO × 5 inch DP S-140 (44 stands) × 5-1/2 inch DP S-140 (21 stands) × 5-1/2 inch DP S-150 (25 stands) × XO × 6-5/8 inch DP Z-140
C000P	LWD/MWD	1939.0	2100.0	4067.5	3058.5	5026.0	12-1/4	Bit × PDM × float sub (non-ported) × 12-1/4 inch stab × AFR × M5 (AGR + EWR + PWD + HCIM) × X-BAT × HOC × 8-1/2 inch DC (12) × drilling jar × XO × 5.68 inch HWDP (12) × XO × 5 inch DP S-140 (65 stands) × 5-1/2 inch DP S-140 (21stands) × XO × 5-1/2 inch DP S-150 (15 stands) × XO × 6-5/8 inch DP Z-140
C000P	Underreamer	1939.0	1936.5	3904.0	2960.5	4928.0	12-1/4, 14-1/2	Bit × bit sub × 14-1/2 inch Anderreamer × float sub (w/flapper-type float) × 8-1/2 inch DC (1) × 12-3/16 inch × 8-1/2 inch DC (11) × drilling jar × XO × 5.68 inch HWDP (12) × XO × 5 inch DP S-140 (67 stands) × 5-1/2 inch DP S-140 (21 stands) × XO × 5-1/2 inch DP S-150 (8 stands) × XO × 6-5/8 inch DP X-140
C000P	Underreamer	1939.0	1936.5	3904.0	2960.5	4928.0	12-1/4, 14-1/2	Bit × bit sub × 14-1/2 inch Anderreamer × float sub (w/flapper-type float) × 8-1/2 inch DC (1) × 12-3/16 inch stab × 8-1/2 inch DC (11) × drilling jar × 8-1/2 inch DC (2) × XO × 5.68 inch HWDP (12) × XO × 5 inch DP S-140 (67 stands) × 5-1/2 inch DP S-140 (21 stands) × XO × 5-1/2 inch DP S-150 (25 stands) × XO × 6-5/8 inch DP Z-140
C000P	Underreamer	1939.0	1936.5	3904.0	2964.5	4932.0	12-1/4, 14-1/2	Bit × bit sub × 14-1/2 inch Anderreamer × float sub (w/flapper-type float) × 8-1/2 inch DC (1) × 12-3/16 inch stab × 8-1/2 inch DC (11) × drilling jar × 8-1/2 inch DC (2) × XO × 5.68 inch HWDP (12) × XO × 5 inch DP S-140 (67 stands) × 5-1/2 inch DP S-140 (21 stands) × XO × 5-1/2 inch DP S-150 (13 stands) × XO × 6-5/8 inch DP Z-140
C000P	Casing run	1939.0	NA	NA	2922.0	4889.5	NA	11¾ inch casing (G/S × 1 × F/C × 9 × L/C × 30 × 41, total 82 joints) × liner hanger × 5 inch DP (5 stands) × 5-1/2 inch DP S-140 (21 stands) × XO × 5-1/2 inch DP S-150 (25 stands) × XO × XO × 5-7/8 inch DP NK-155 (19 stands)

NA = not applicable. SD-RCB = small-diameter rotary core barrel system, LWD/MWD = logging while drilling/measurement while drilling, WBRRT = wear bushing running/retrieving tool. Stab = stabilizer, DC = drill collar, XO = cross-over sub, HWDP = heavy-wall drill pipe, DP = drill pipe, CST = concentric string tool, DGR = dual gamma ray tool, EWR = electromagnetic wave resistivity tool, PADPRT = pressure-assisted drill pipe running tool, CMT = drill stand, PDM = positive-displacement motor. GVR = geoVISION resistivity tool, ARC8 = arcVISION array resistivity compensated tool, AFR = azimuthal focused resistivity tool, AGR = azimuthal gamma ray tool, DGR = dual gamma ray tool, EWR = electromagnetic wave resistivity tool, PWD = pressure while drilling tool, X-BAT = azimuthal sonic/ultrasonic tool.

Table T5. Casing depths, drilling depths, and significant events, Expedition 348.

Event	Time, Date (h UTC, 2013/2014)	Measured depth (MD; mBRT)	Measured depth (MD; mbsf)	True vertical depth (TVD; mbsf)	Remarks
Sea level		1967.50	0.00	0.00	
36 inch casing		2021.40	53.90	53.90	
20 inch casing		2827.80	860.30	860.30	
Lithologic Unit I/II boundary		2167.50	200.00	200.00	
Lithologic Unit II/III boundary		2843.00	875.50	875.50	
Lithologic Unit III/IV boundary		2943.00	975.50	975.50	
Lithologic Unit IV/V boundary		3633.00	1665.50	1664.40	
TD Hole C0002F		3973.00	2005.50	2005.50	
Hole C0002F side track	0815, 4 Nov	2845.00	877.50	877.50	
Hole C0002N	0815, 4 Nov	2827.80	860.30	860.30	
Borehole conditioning (top)	1030, 6 Nov	2805.90	838.40	838.40	*1205–1221 mbsf; ~15 h
Borehole conditioning (bottom)	2245, 5 Nov	3186.50	1219.00	1217.90	*1205–1221 mbsf; ~15 h
WOW #1	2115, 7 Nov	3645.00	1677.50	1676.40	POOH to 1939.8 mBRT
WOW #1	2200, 8 Nov	3645.00	1677.50	1676.40	*1662–1678 mbsf; ~28.5 h
Lost signal	0815, 9 Nov	3823.80	1856.30	1855.20	
WOW #2	0000, 10 Nov	3976.00	2008.50	2007.40	POOH to surface
WOW #2	2215, 11 Nov	3976.00	2008.50	2007.40	*1992–2008 mbsf; ~50 h
Mud loss #1	2345, 11 Nov	4004.00	2036.50	2035.40	*2022–2038 mbsf; ~8.5 h
Mud loss #1	0000, 12 Nov	3995.50	2028.00	2026.90	*2022–2038 mbsf; ~8.5 h
Mud loss #2	1100, 12 Nov	4085.00	2117.50	2116.40	
Hole C0002N TD	0115, 13 Nov	4297.50	2330.00	2328.90	859.5–2329.3 (1962.6–2008.5 overlap zone) mbsf; logged interval
Hole C0002N 13-3/8 inch casing	0645, 22 Nov	3977.50	2010.00	2008.90	2013 m total length
13-3/8-inch casing TOC		3320.00	1352.50	1351.41	
Bridge plug	1745, 7 Dec	3916.50	1949.00	1947.90	
Top of DC fish		3928.08	1960.58	1959.50	
Window top		3904.00	1936.50	1935.40	
Window bottom		3912.63	1945.13	1944.00	
Hole C0002P sidetrack top	0000, 15 Dec	3904.00	1936.50	1935.40	
LOT #1	0630, 15 Dec	3922.00	1954.50	1953.40	1130 psi (7.79 Mpa)
LOT #2	0700, 15 Dec	3922.00	1954.50	1953.40	1280 psi (8.83 Mpa)
WOW #3	18–20, Dec	4035.20	2067.70	2066.50	
Bottom of kickoff	1400, 20 Dec	4075.00	2107.50	2106.30	
Core prep	20–22, Dec	4130.50	2163.00	2161.70	
Top RCB coring	2045, 22 Dec	4130.50	2163.00	2161.70	
Fault zone		4172.50	2205.00		Zone width: 2204.9–2205.8 mbsf
Bottom of RCB coring	1745, 24 Dec	4186.00	2218.50	2216.60	
Open hole (top)	1200, 27 Dec	4130.00	2162.50	2161.20	*2163–2218.5 mbsf; >66.25 h
Open hole (bottom)	1800, 27 Dec	4186.00	2218.50	2217.10	*2163–2218.5 mbsf; >66.25 h
TD 12-1/4 inch LWD	0700, 1 Jan	5026.00	3058.50	3056.60	2163.5–3058.5 mbsf; logged interval
Top of open hole 14½ inch	2230, 2 Jan	3928.00	1960.50	1959.40	
Stuck pipe	1340, 11 Jan	4928.00	2960.50	2959.50	2960.5 mbsf; ~1.75 h
Stuck pipe	0400, 14 Jan	4932.00	2964.50	2963.50	2964.5 mbsf; ~17 h; pressure stabilized at 15.2 Mpa
Hole C0002P 11¾ inch casing	0630, 18 Jan	4890.00	2922.50	2920.65	1007.18 m total length
LOT #3	1945, 19 Jan				After diverter, before CRT; 650 psi (4.48 Mpa) and 530 psi (3.65 Mpa)
TD 14-1/2 inch hole		4927.50	2960.00	2958.14	

* = depth intervals with long exposure time before LWD tools were able to log after initial drilling. TD = total depth, WOW = waiting on weather, TOC = top of casing/cement, DC = drill collar, LOT = leak-off test, RCB = rotary core barrel, LWD = logging while drilling, POOH = pull out of hole, CRT = casing running tool.

Figure F1. A. Map of the NanTroSEIZE region showing all Stage 1, 2, and 3 drill sites. Red = Expedition 348 Site C0002, white = other NanTroSEIZE sites. Black outline = region with 3-D seismic data, yellow arrows = estimated far-field vectors between Philippine Sea plate and Japan (Seno et al., 1993; Heki, 2007). Stars = epicenter locations of 1944 and 1946 tsunamigenic earthquakes. **B.** Bathymetric map showing all Site C0002 holes. The long-term borehole monitoring system is installed in Hole C0002G, and the riser hole is Hole C0002F/C0002N/C0002P. The lines from Hole C0002F show the azimuth and deflection of Holes C0002N (blue dashed line) and C0002P (green line) from the original Hole C0002F borehole.

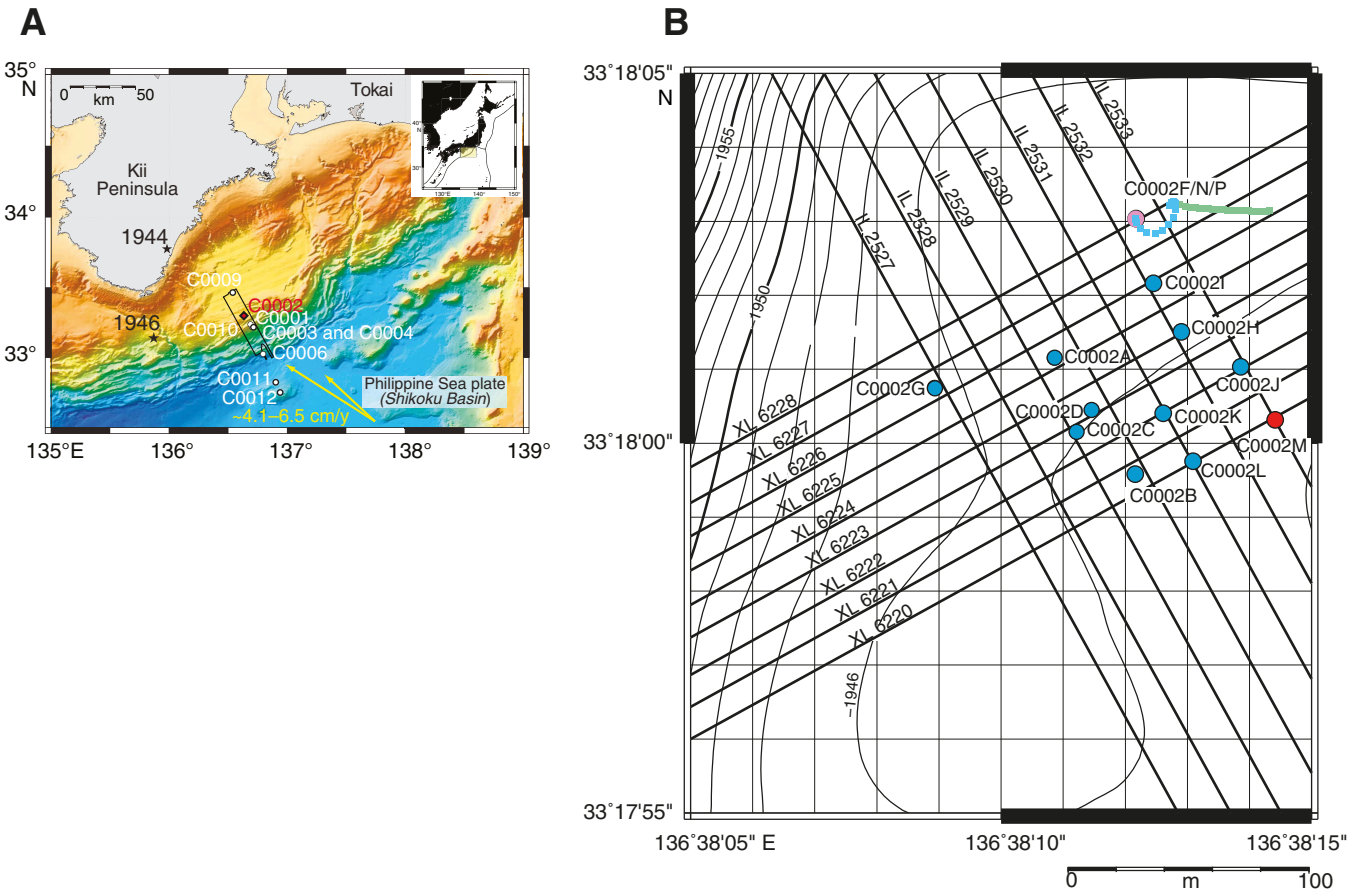

Figure F2. Composite seismic reflection depth section extracted from the pre-stack depth migrated 3-D seismic volume, showing position of Site C0002 (red) and other NanTroSEIZE sites (black). **A.** Seismic section in the region around Holes C0002F, C0002N, and C0002P. The heavy solid red line represents the currently drilled borehole, and the dashed line shows the projected extension to the plate boundary fault target. The boxes represent cased sections of Holes C0002F, C0002N, and C0002P (red shows the 36 and 20 inch casing, green represents the 13⅜ inch casing, and blue indicates the 11¾ inch casing liner section. **B.** Composite seismic depth section of the NanTroSEIZE site and related drilling sites from the Kumano Basin (Site C0009) to the input sites (C0011 and C0012).

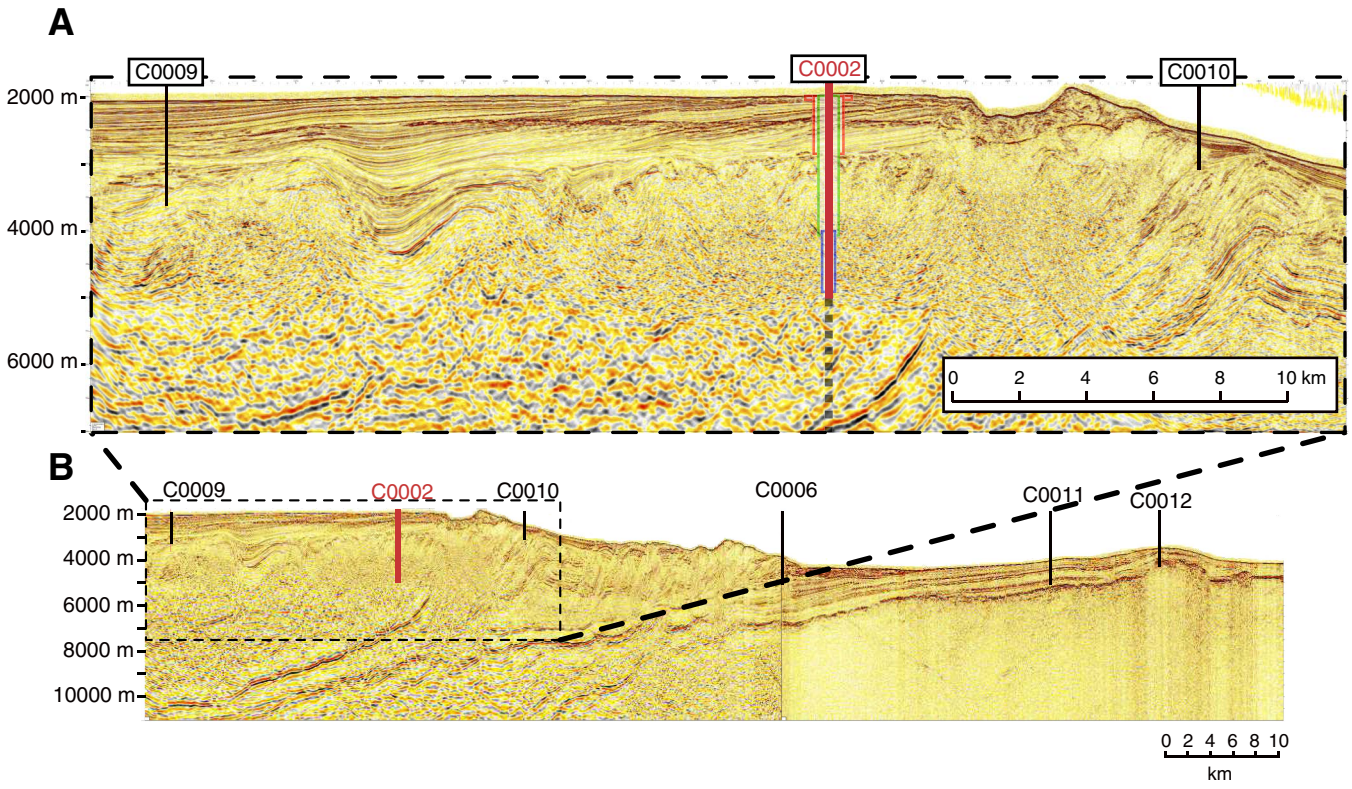

Figure F3. Hole C0002F, C0002N, and C0002P casing and depth schematic overlain on inline seismic Section 2529 from the pre-stack depth migrated 3-D seismic volume. The horizontal scale does not allow display of the Hole C0002N and C0002P sidetrack offset. The black line represents the borehole, with the final target (red arrowhead) intersecting the plate boundary fault (blue dashed lines). The bottom simulating reflector (BSR) is shown by the opaque blue dashed line. The boundary between forearc basin sediment and accretionary prism is represented by the dashed purple line. The black outlined gray box indicates the current borehole, with casing depths indicated by the green arrowheads. The blue stippled box indicates the cored section of Hole C0002P. LWD = logging while drilling.

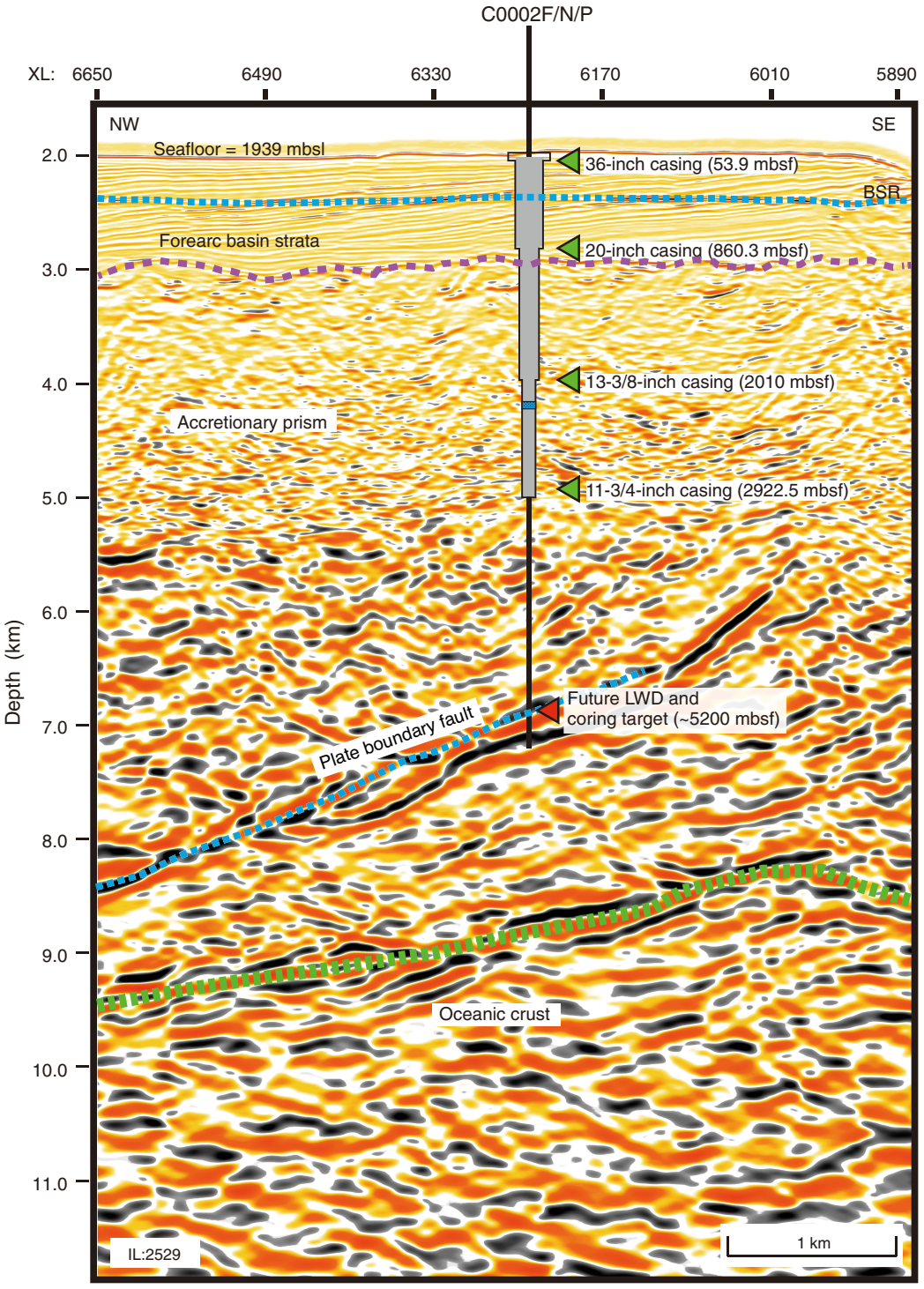

Figure F4. Summary diagram of all drilling and coring at Site C0002. Cored sections are indicated by the brown lines, yellow indicates the observatory, green indicates logging-while-drilling sections, and black indicates sections that were drilled without any sampling. The transect for these holes follows inline seismic Section 2529. The blue dashed line schematically indicates the approximate upper limit of the accretionary prism.

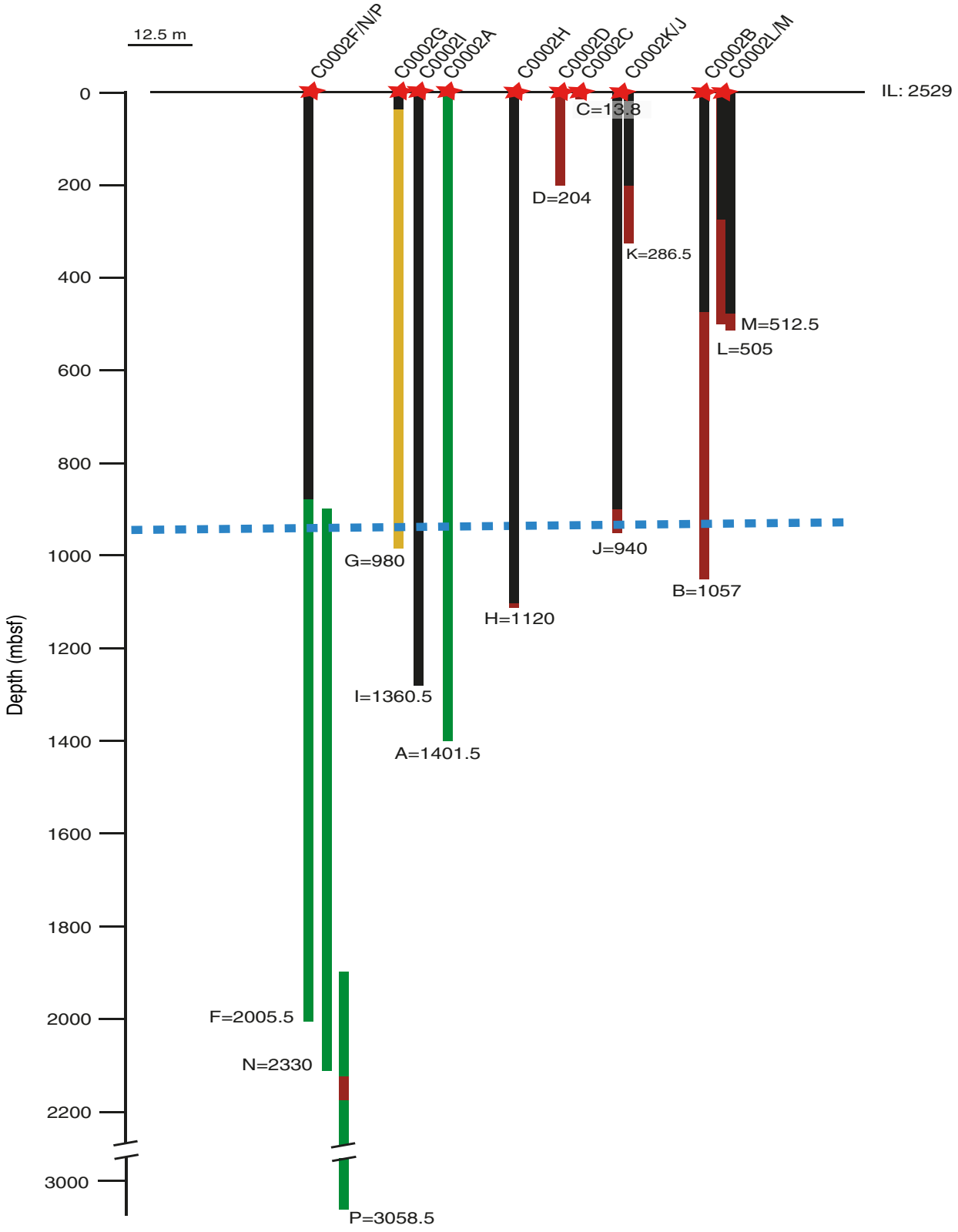

Figure F5. Composite summary plot of data from multiple expeditions and phases of drilling at Site C0002. Resistivity image and logging-while-drilling logs are from Holes C0002F, C0002N, and C0002P. Logging and lithologic unit boundaries are from Expeditions 315, 338, and 348. Percent ratios of cuttings samples from Holes C0002N and C0002P are also shown.

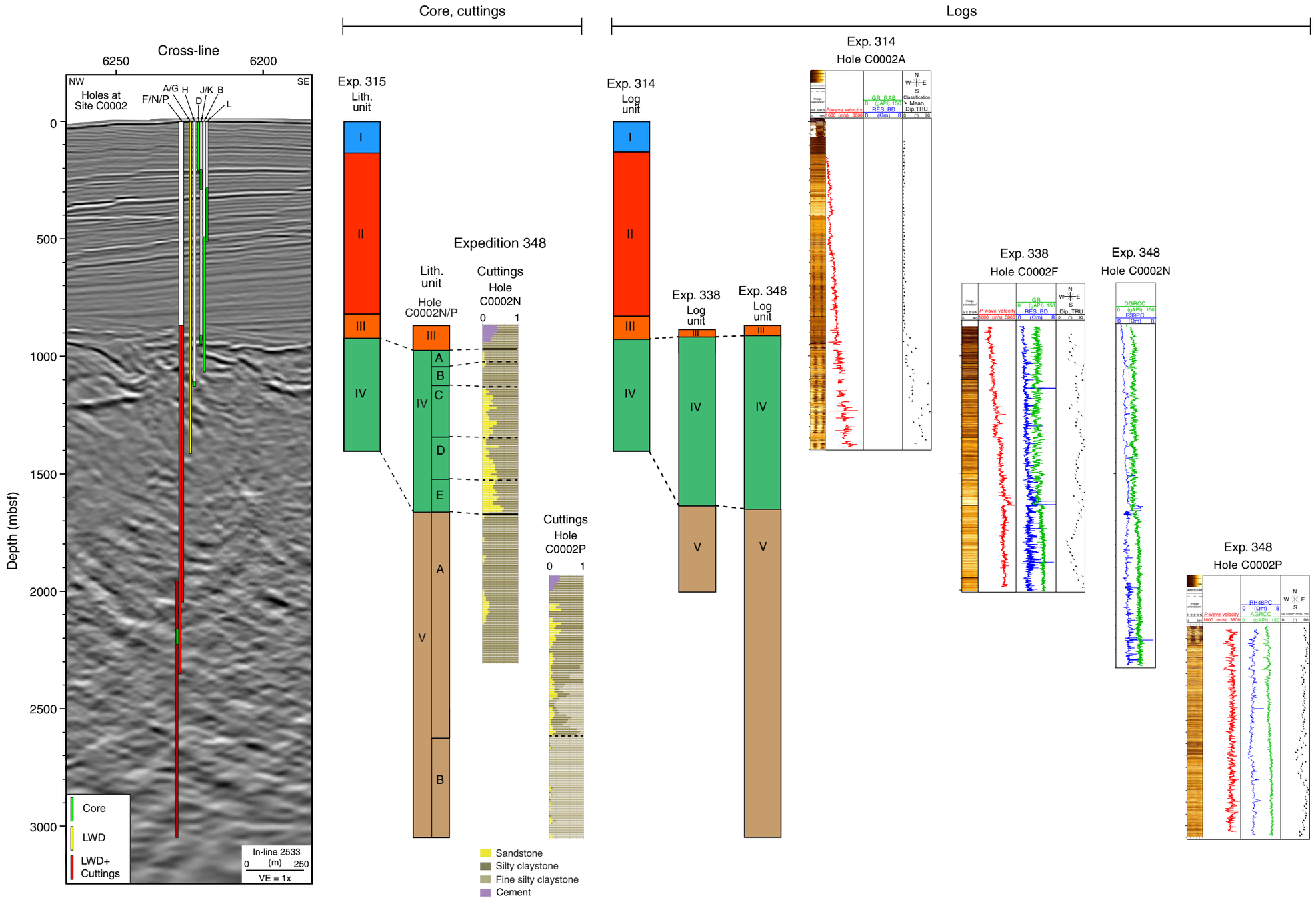

Figure F6. Visual estimation of lithologic composition of cuttings, sampled every 5 m, with associated lithostratigraphic unit designations. **A.** Hole C0002N. (Continued on next two pages.)

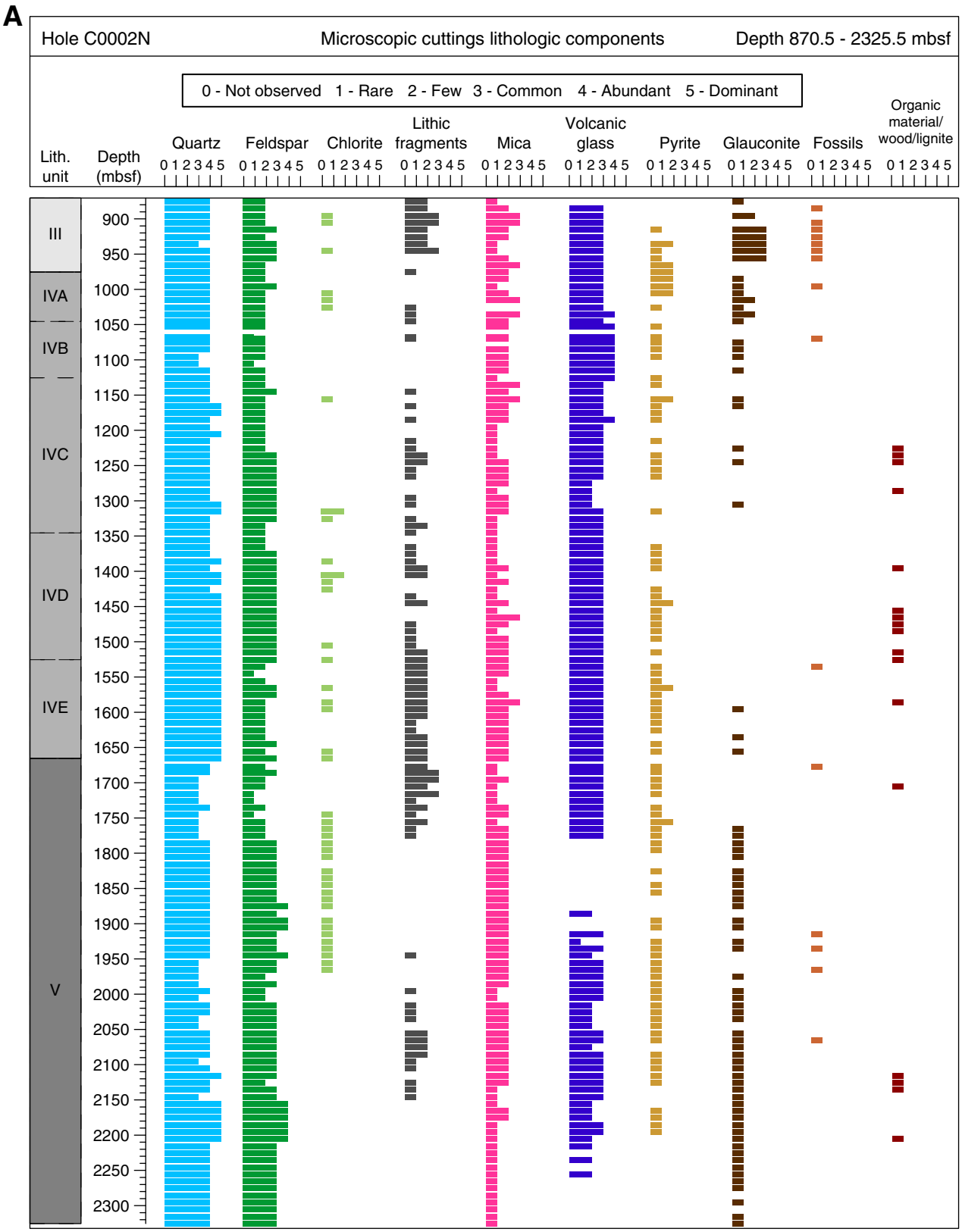

Figure F6 (continued). B. Hole C0002P. (Continued on next page.)

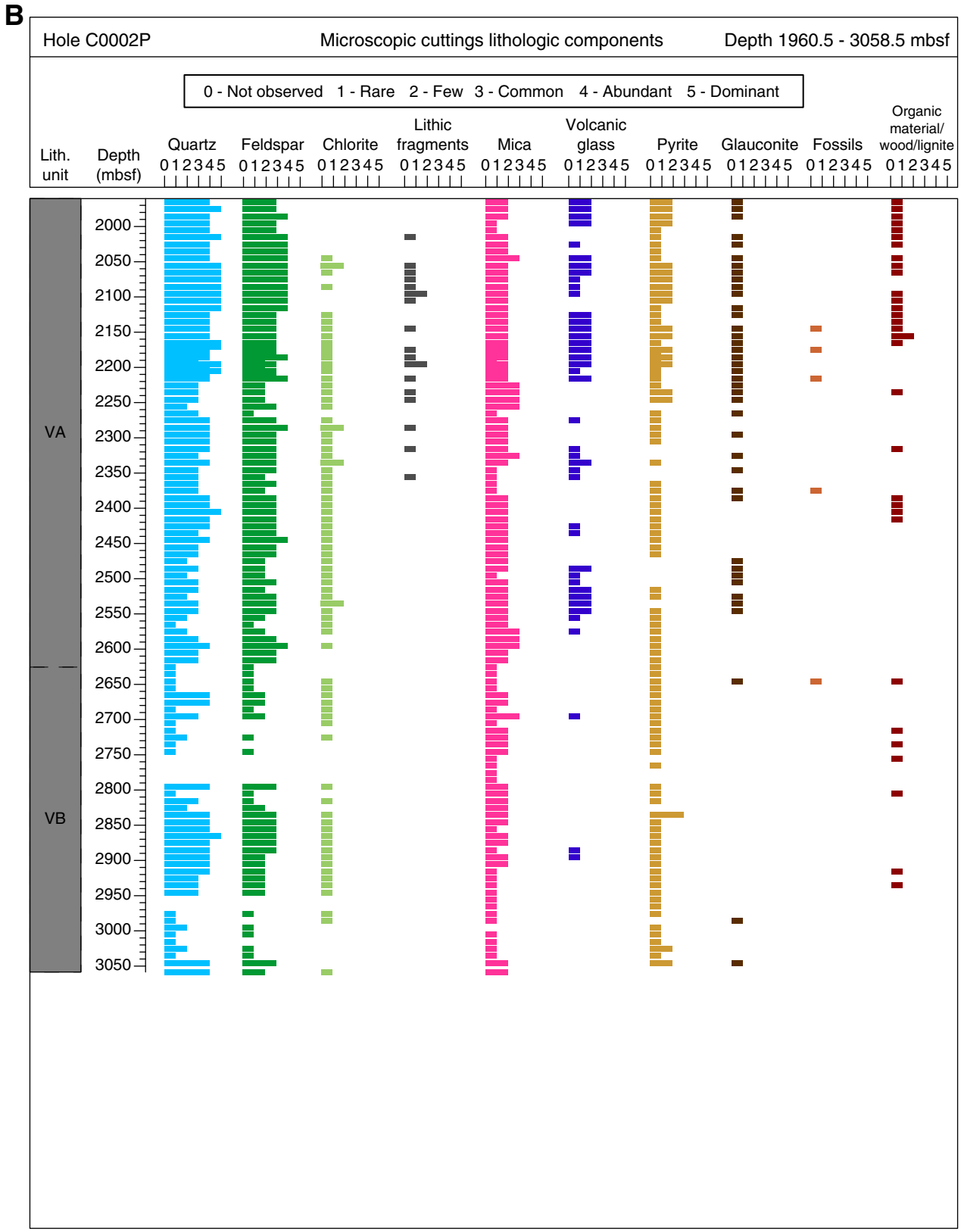

Figure F6 (continued). C. Hole C0002P coring interval smear slides.

Figure F7. Summary of structural observations based on hand-selected intact cuttings, Holes C0002N and C0002P. **A.** >4 mm size fraction. **B.** 1–4 mm size fraction.

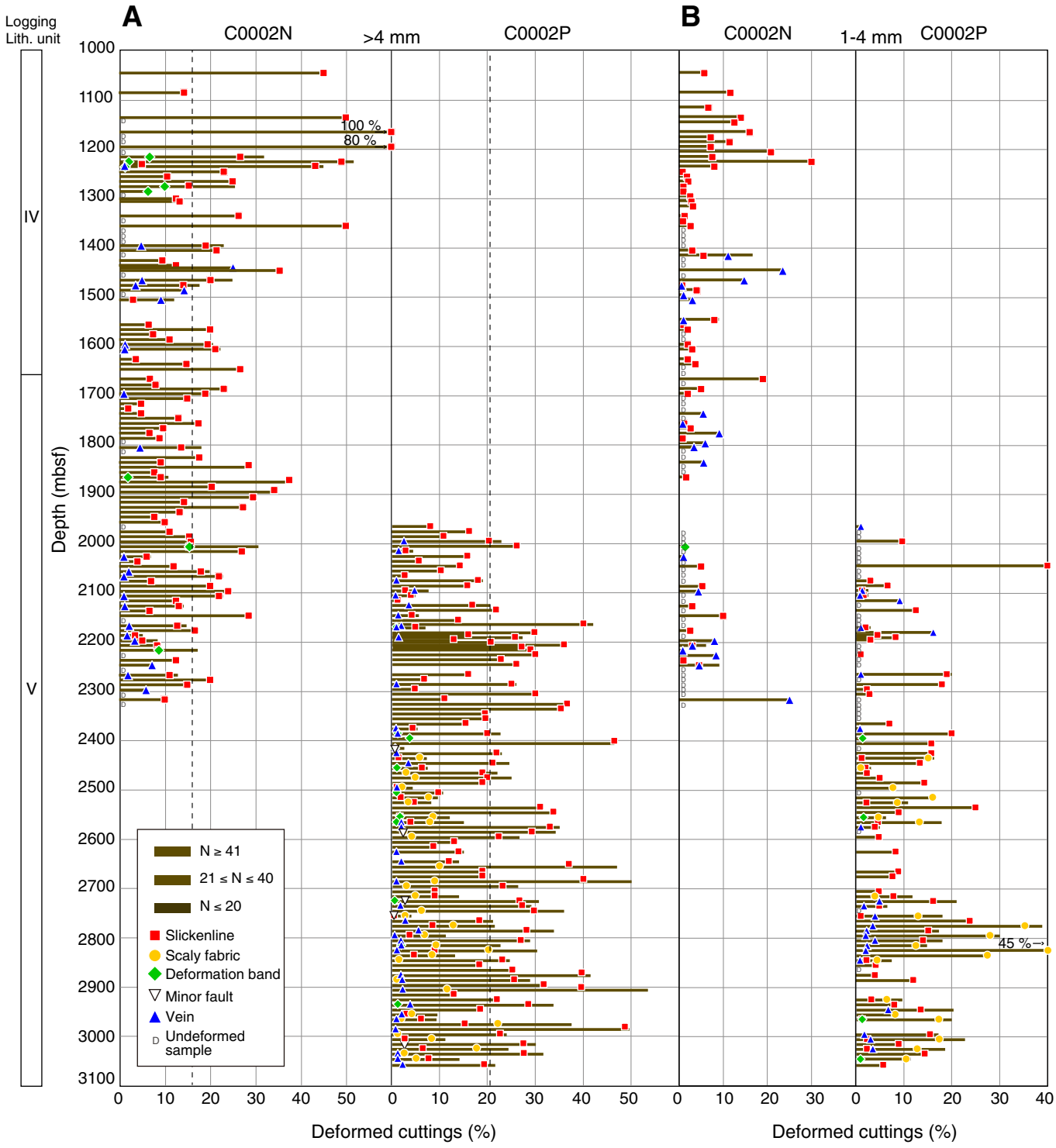

Figure F8. Depth distribution of dip angle variation, Hole C0002P. **A.** Bedding. **B.** Minor faults, veins, and deformation bands.

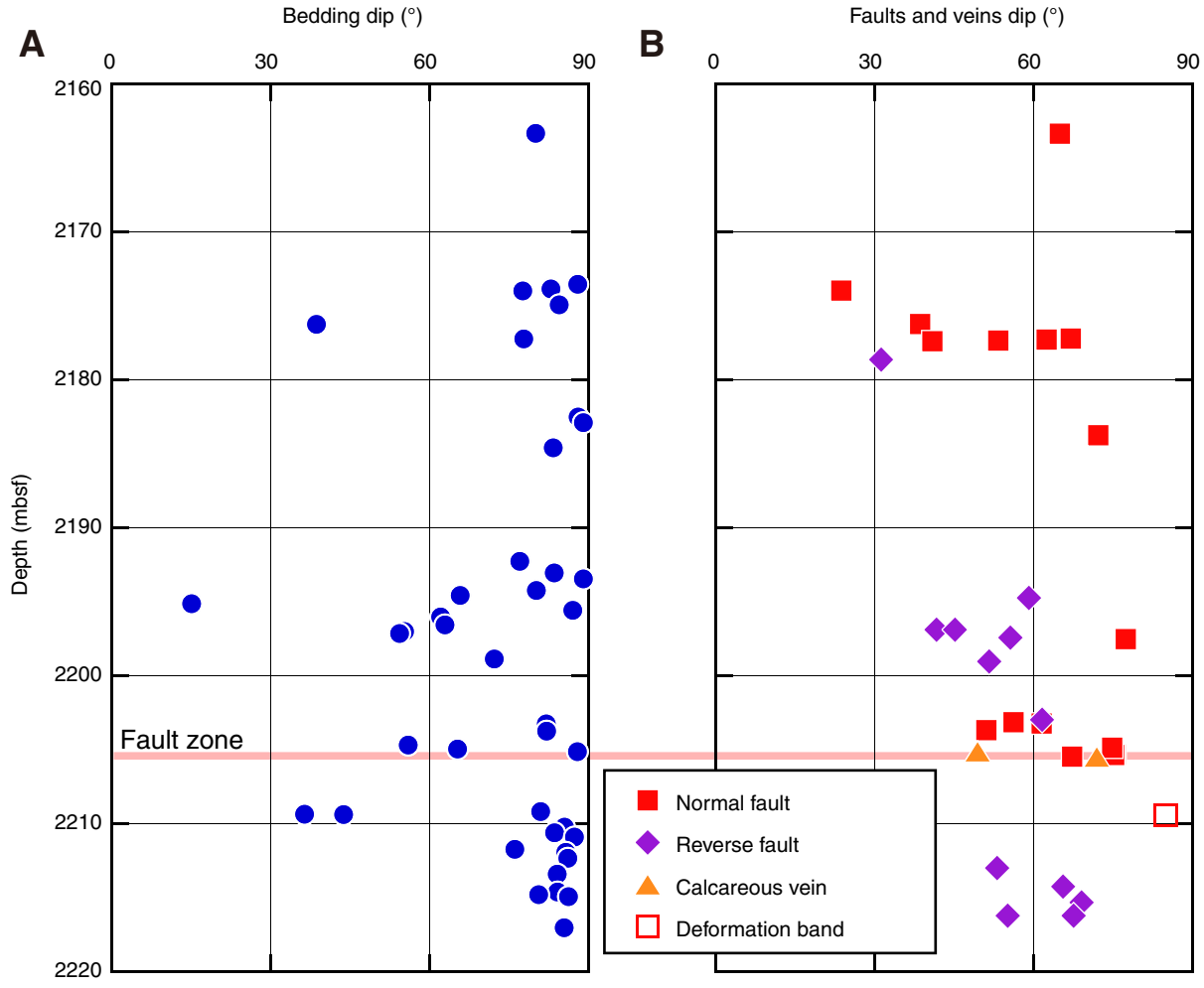

Figure F9. A. Slickenlines/steps on the surface of carbonate vein (Sample 348-C0002P-242-SMW; 2800.5 mbsf). **B.** Deformation band in intact cuttings (Sample 348-C0002N-220-SMW; 1860.5 mbsf). **C.** Photomicrographs of minor fault array (Sample 348-C0002P-151-SMW; 2410.5 mbsf). **D.** Scaly fabric (Sample 348-C0002P-157-SMW; 2430.5 mbsf). **E.** Part of the fault zone in cores retrieved from Section 348-C0002P-2R-4 (2205.22–2205.58 mbsf; working half). **F.** Enlargement of image in E.

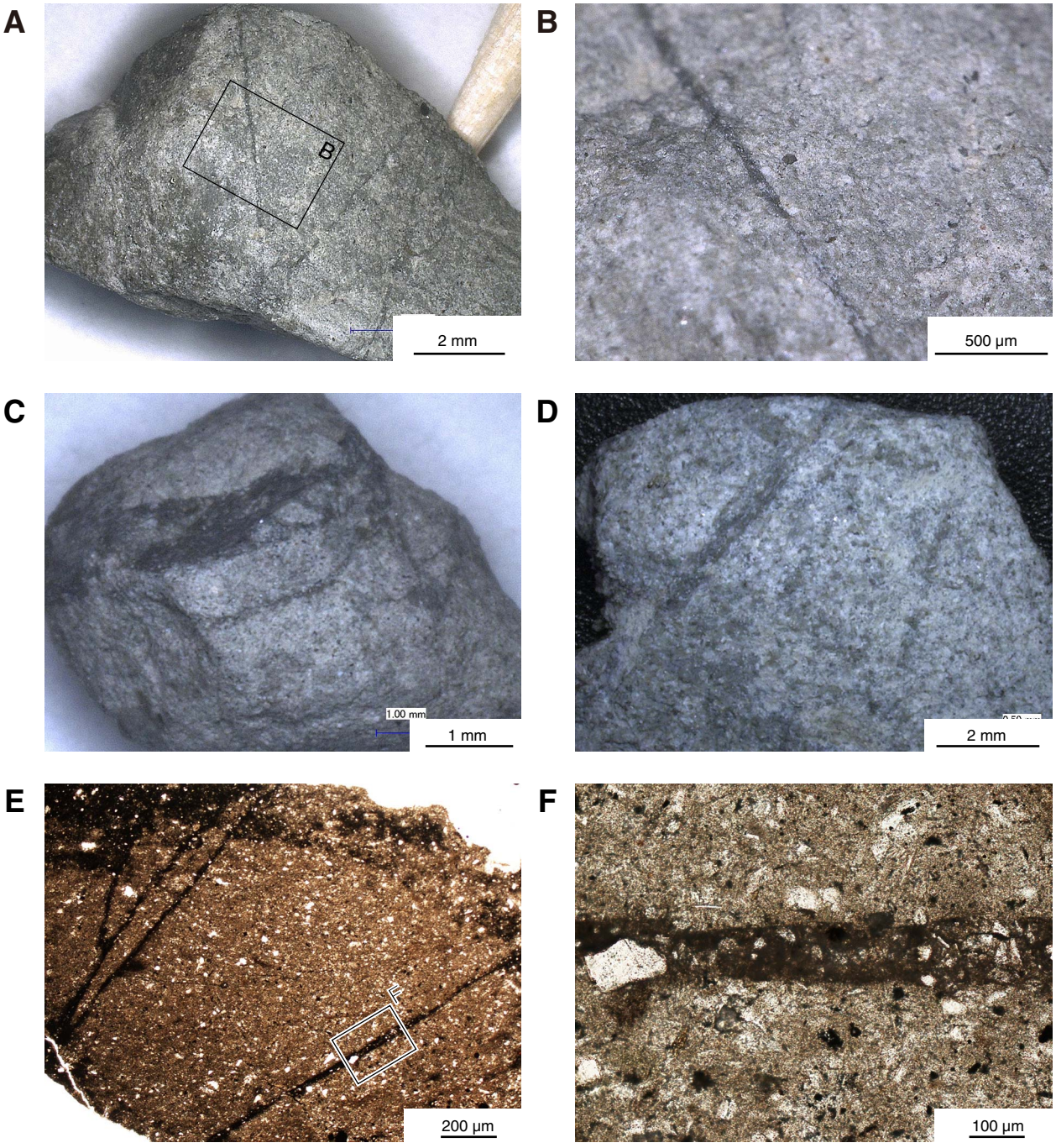

Figure F10. Nannofossil ranges presented as age-depth chart. Bedding dips vary between 60° and 90° and sediment is strongly deformed, so this information does not imply a mass accumulation rate. In Hole C0002P, diagnostic information is very limited, with poor preservation of calcareous fossils, perhaps because steep dips mean little stratigraphy was traversed; however, this data is broadly consistent with depositional ages between 9.56 and 10.73 Ma. LO = last occurrence, FCO = first common occurrence, FO = first occurrence.

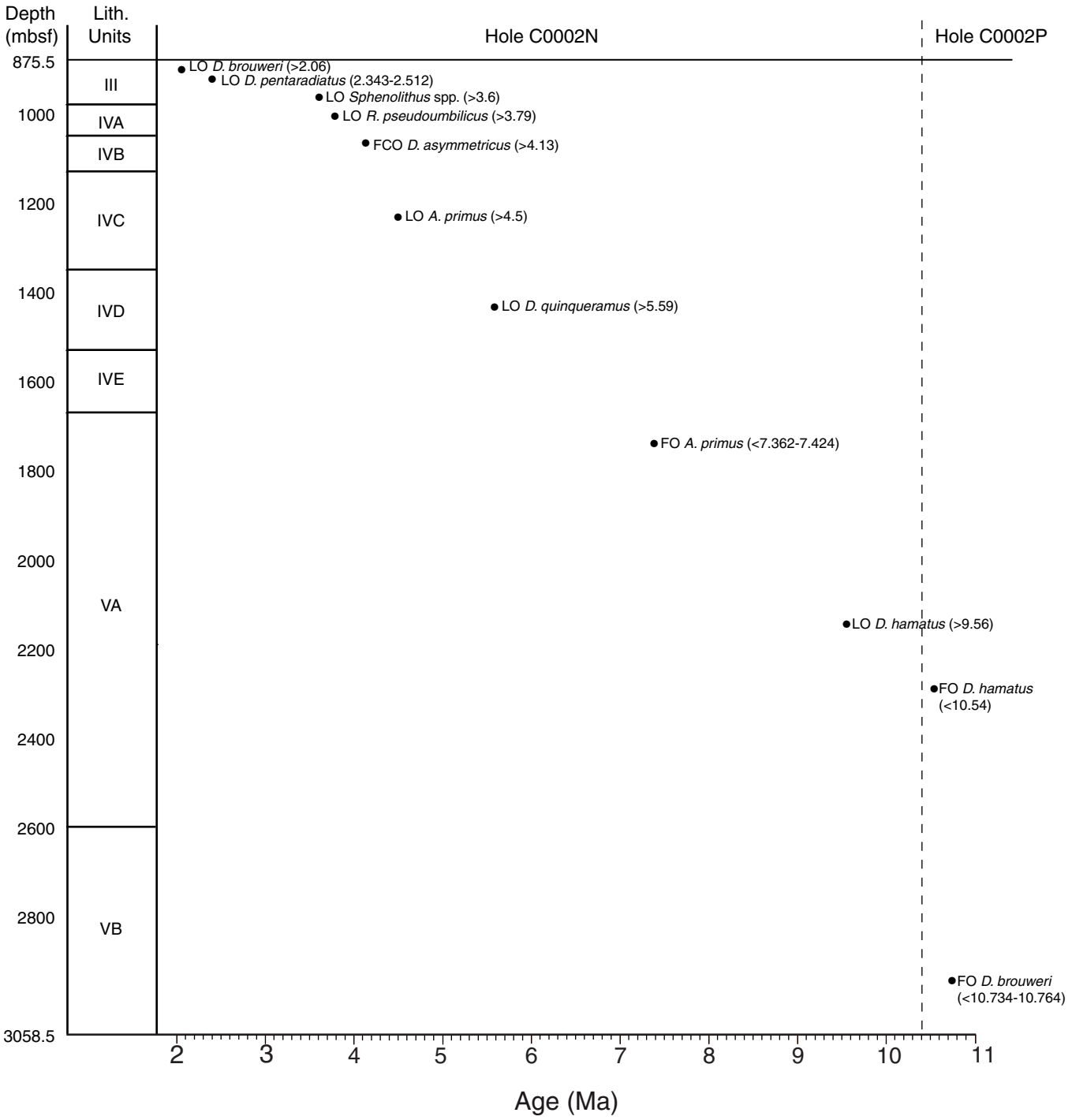

Figure F11. A, D. Normalized change in intensity. **B, E.** Lower hemisphere equal area projection. **C, F.** Progressive alternating field (AF) demagnetization displayed by vector endpoint diagram. Data points = magnetization vector for individual demagnetization steps projected onto horizontal and vertical plane. Figures were prepared with PuffinPlot (Lurcock and Wilson, 2012).

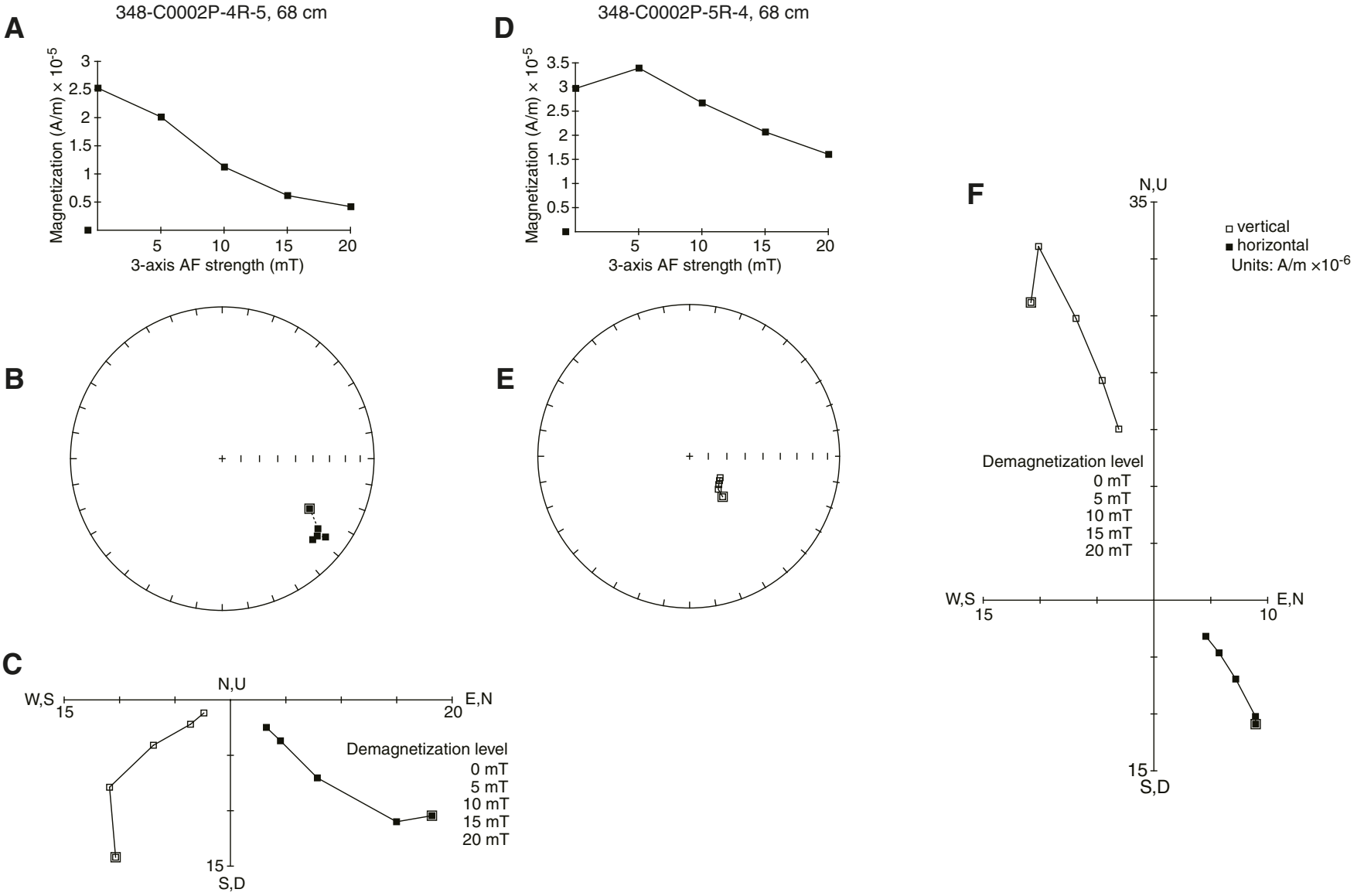

Figure F12. Paleomagnetic inclination, declination, and intensity after 20 mT demagnetization, Hole C0002P. Blue shading = brittle fault zone (2204.9–2205.8 mbsf).

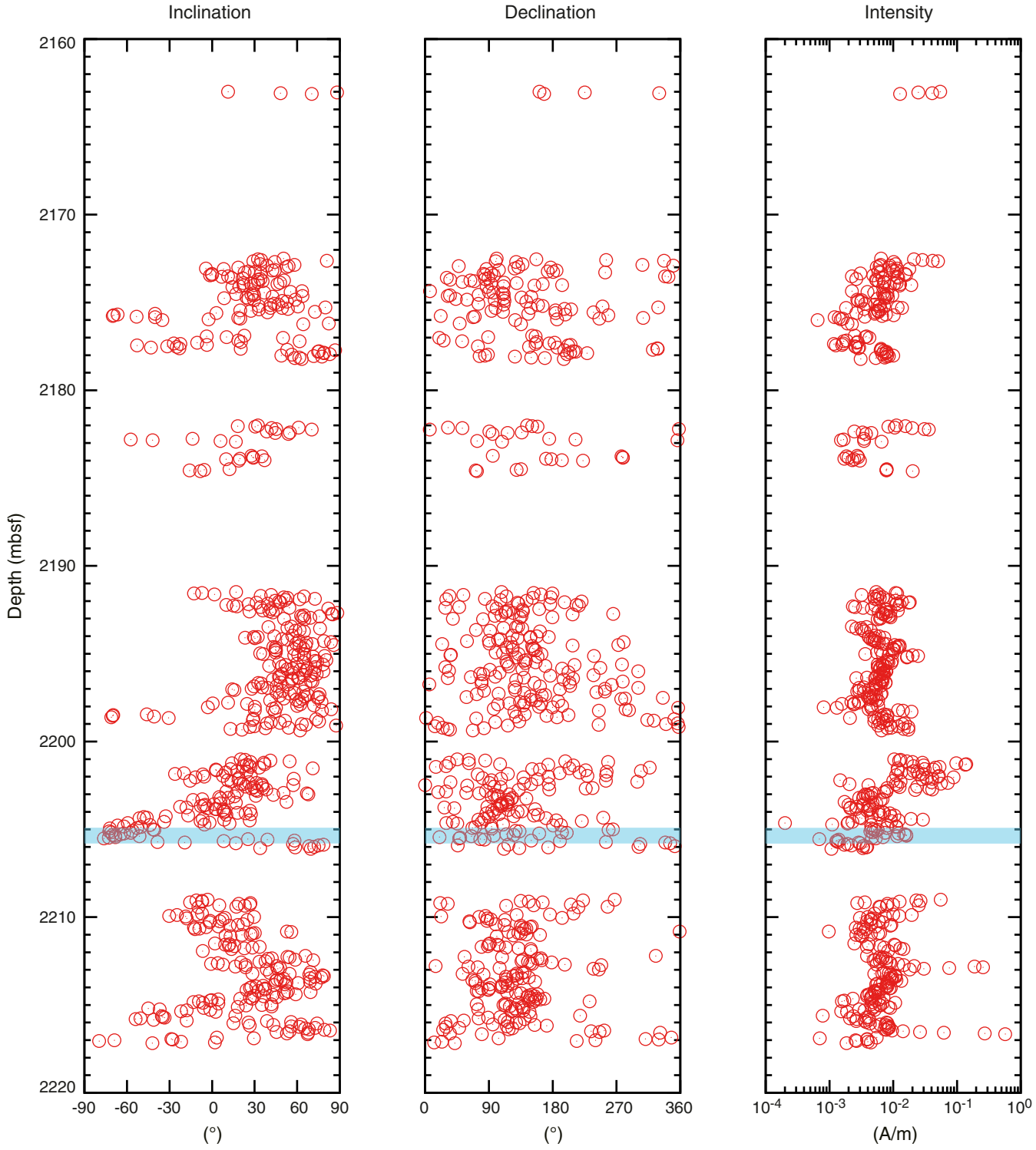

Figure F13. Chlorinity, Hole C0002M. Measured chlorinity values for different squeezing pressure steps are shown. Data represent separate water aliquots from sequential squeeze steps.

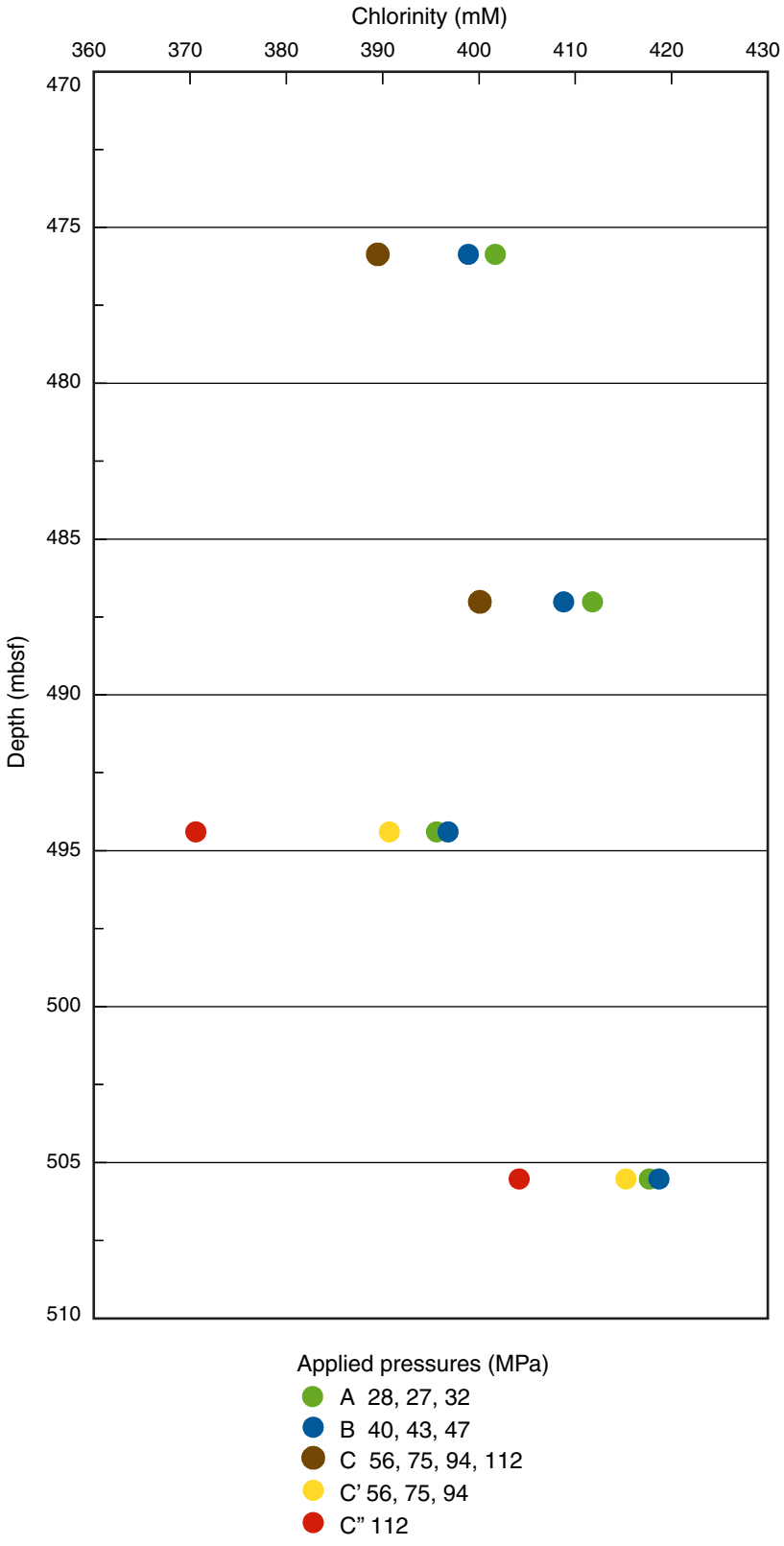

Figure F14. Salinity, pH, and downhole concentrations of chlorinity, bromide, sulfate, and ammonium determined by the GRIND method, Hole C0002P.

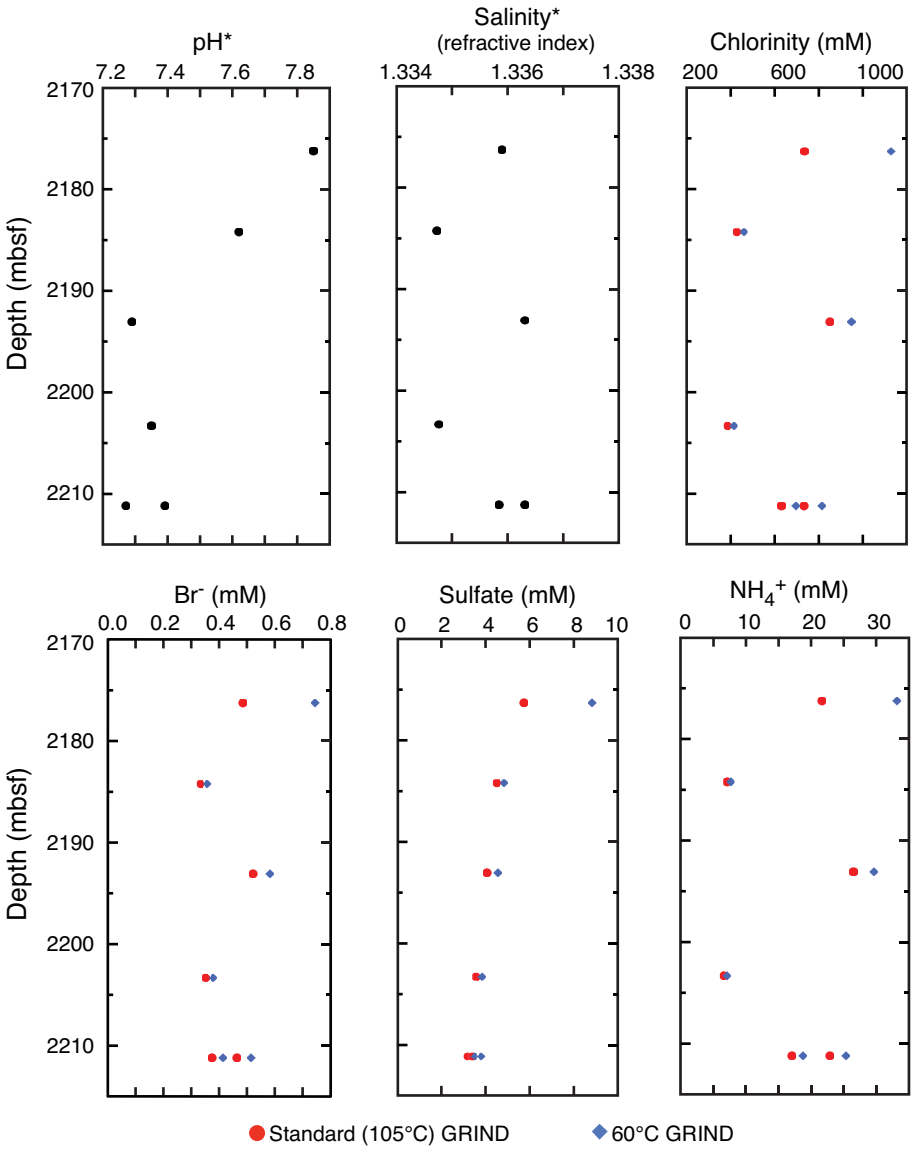

Figure F15. Carbonate, total organic carbon (TOC), and total nitrogen (TN), Holes C0002N and C0002P.

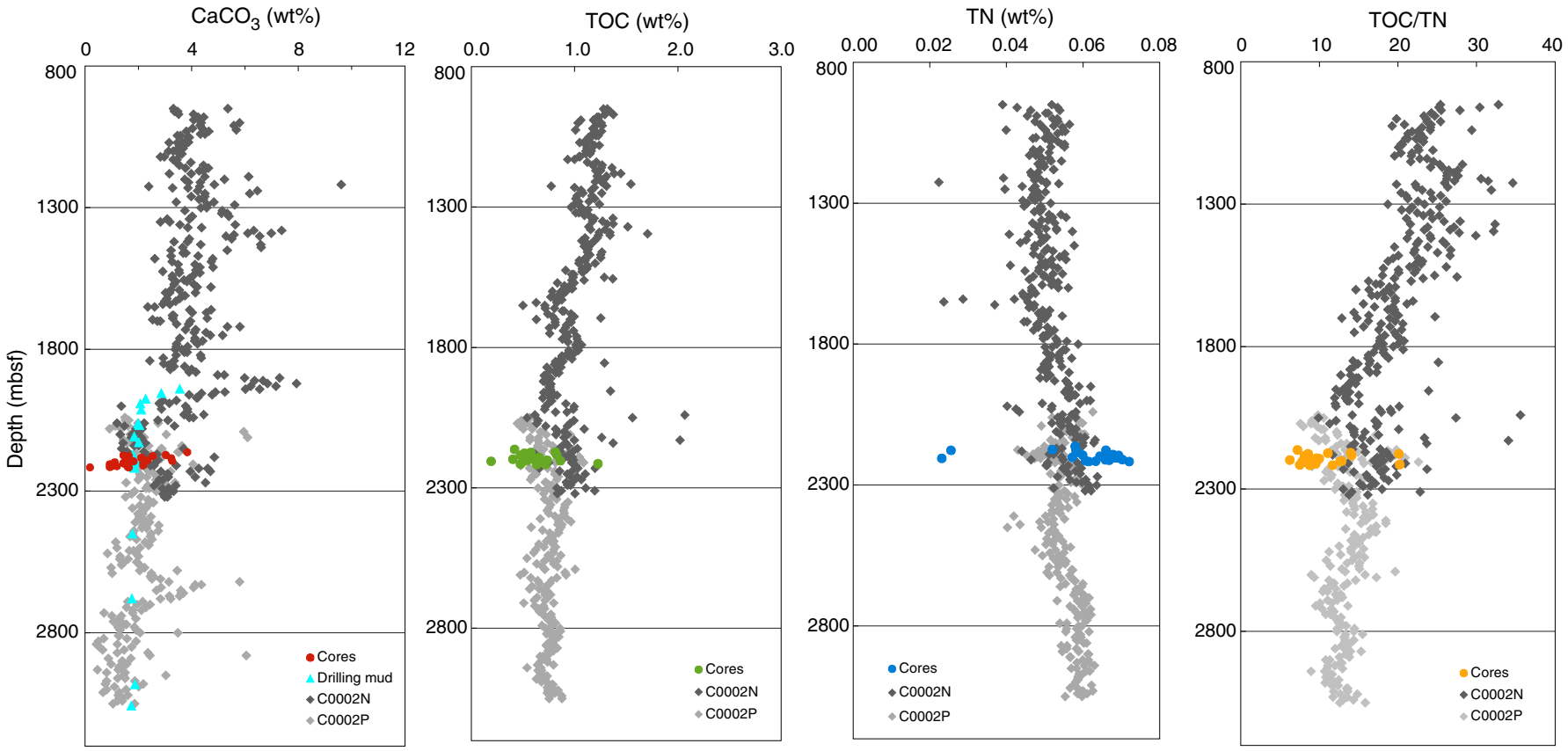

Figure F16 A. Total gas, methane, ethane, and propane in mud gas, Holes C0002F, C0002N, and C0002P. **B.** Bernard plot ($C_1/[C_2 + C_3]$) vs. carbon isotopes of methane gas for mud gas and headspace gas, Holes C0002N and C0002P.

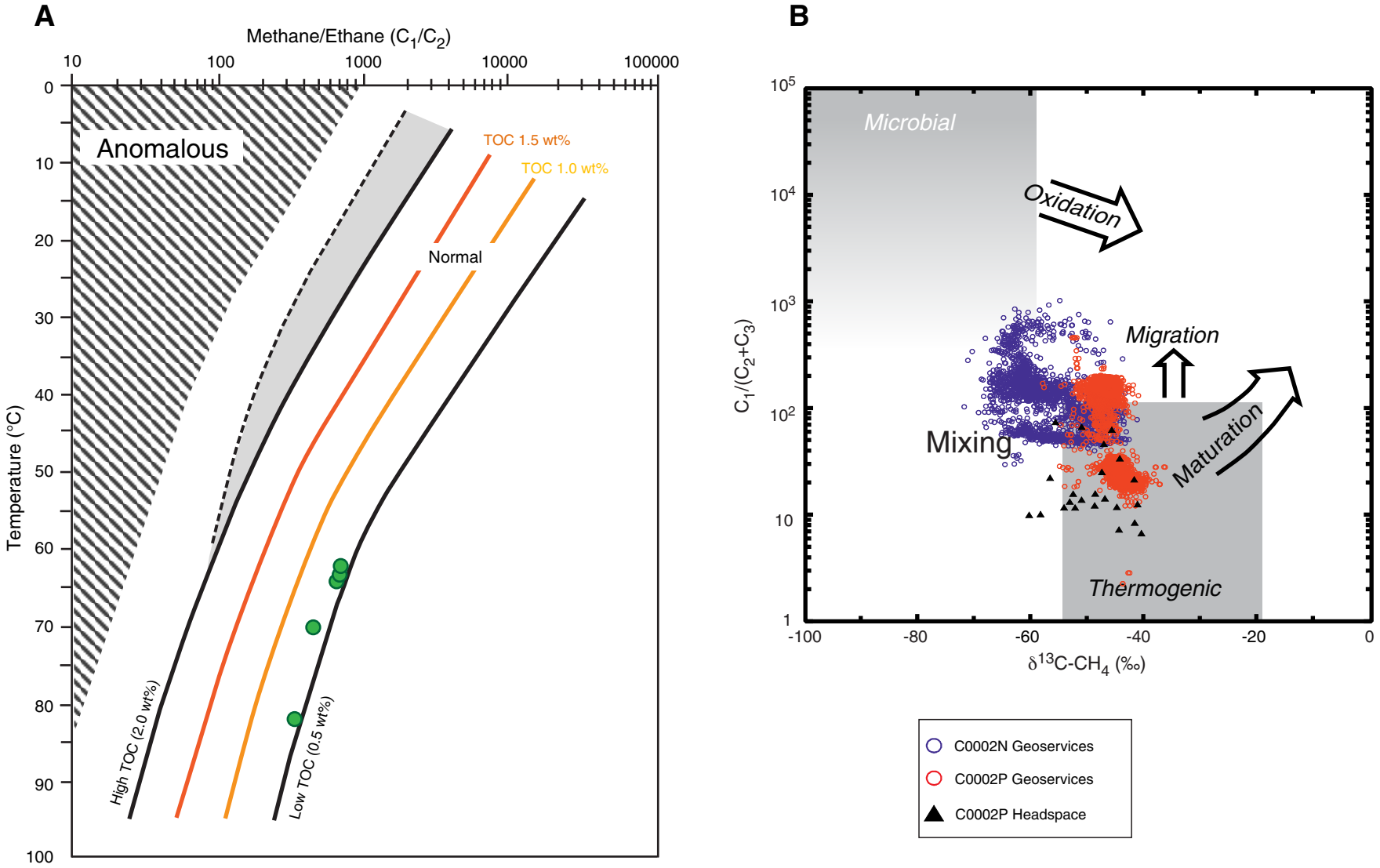

Figure F17. Physical properties measurements on 1–4 and >4 mm cuttings, Holes C0002N and C0002P. **A.** Grain density. **B.** Bulk density. **C.** Porosity. **D.** Electrical conductivity. **E.** *P*-wave velocity. DICA = drilling-induced cuttings aggregate.

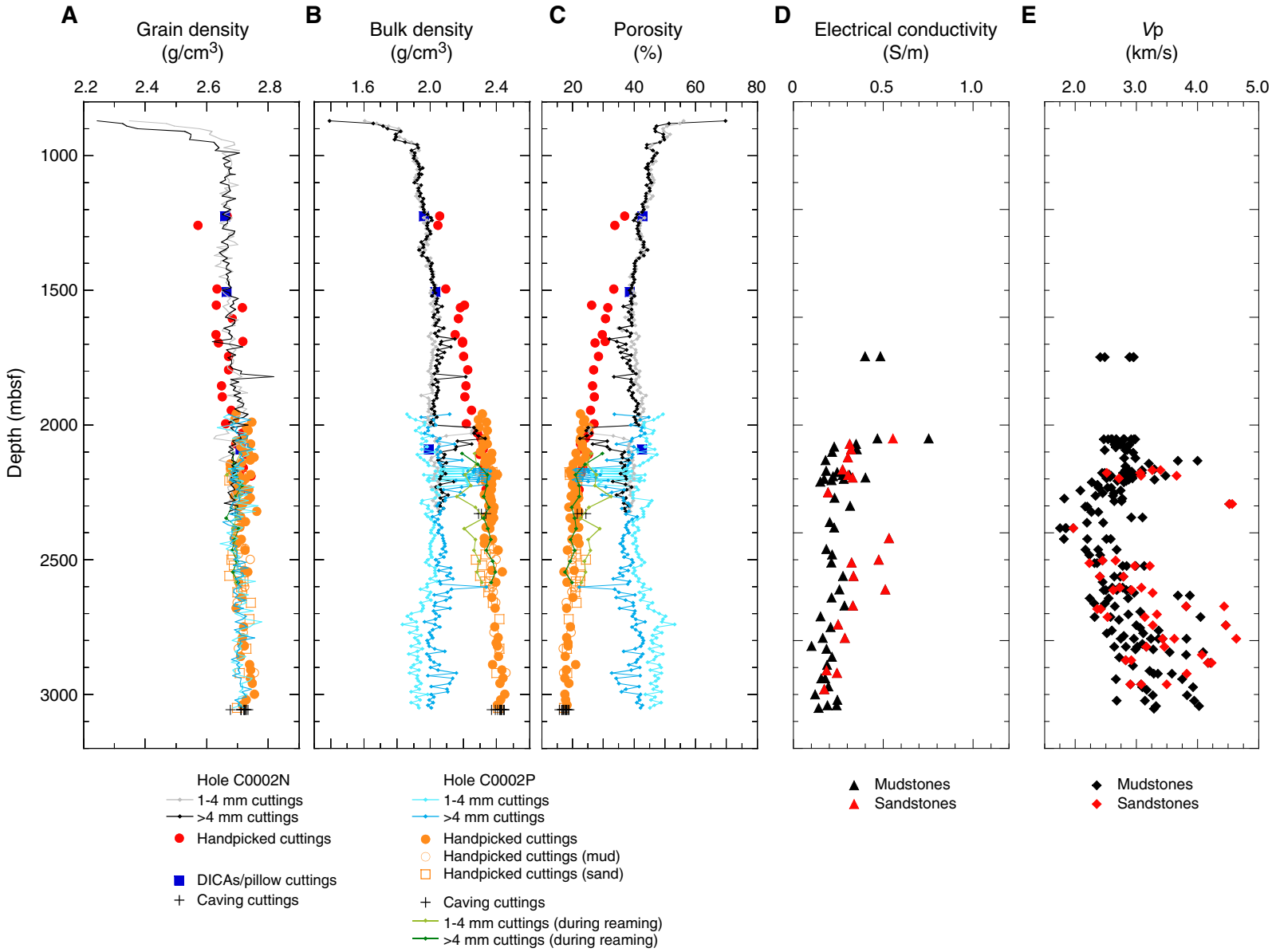

Figure F18. Drilling parameters and selected logs, Holes C0002N and C0002P. PWD = pressure while drilling, EWR = electromagnetic wave resistivity tool, Ph. Resis. = phase resistivity. **A.** Hole C0002N. Exposure time data drawn with dashed lines at ~2000 mbsf was reconstructed because data were not recorded during the changeover from Run 1 to Run 2. (Continued on next page.)

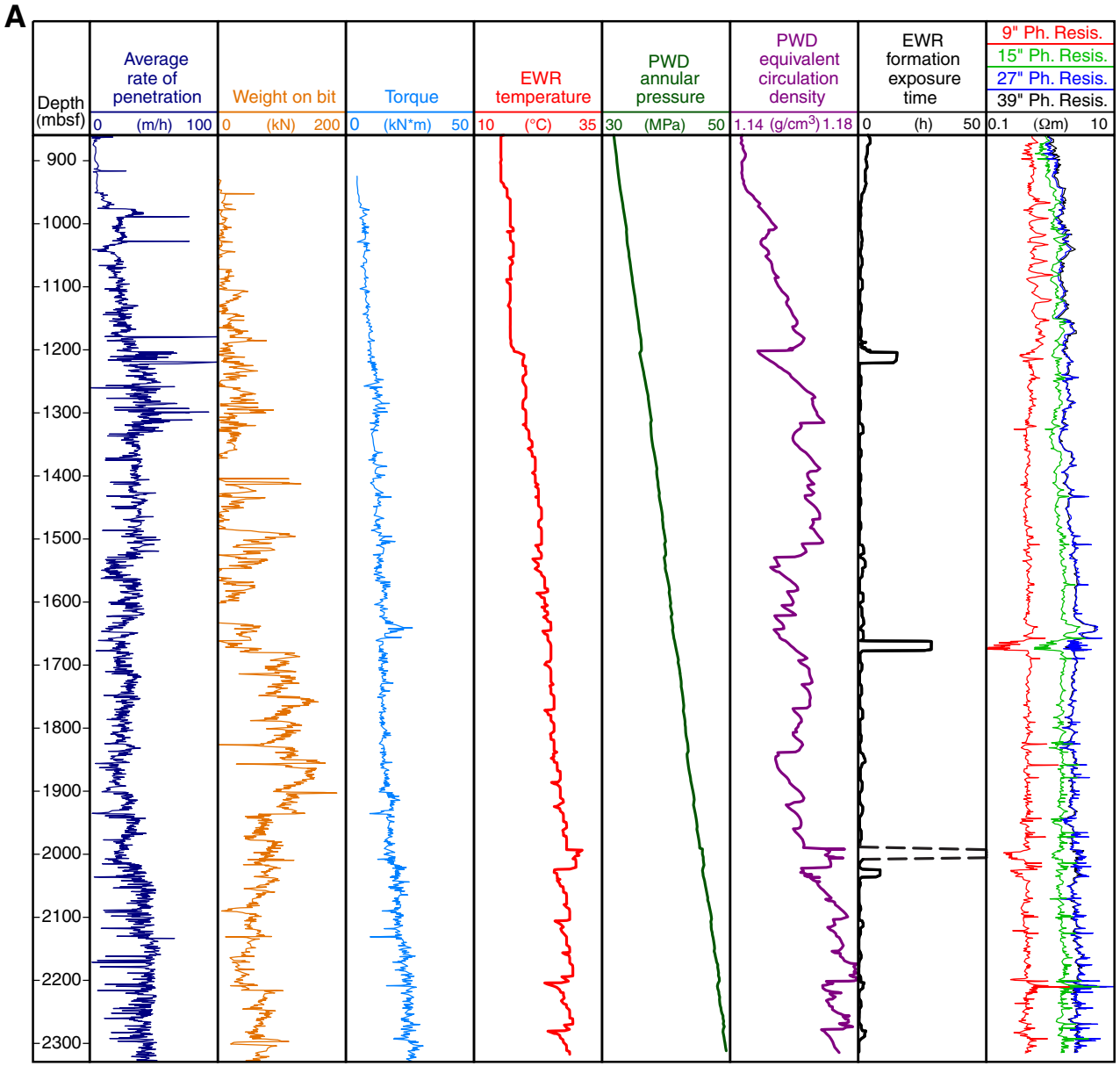

Figure F18 (continued). B. Hole C0002P. The cored interval (2163–2218.5 mbsf) is shown in gray. Ultrasonic caliper data are shown together with a vertical baseline representing the drill bit diameter.

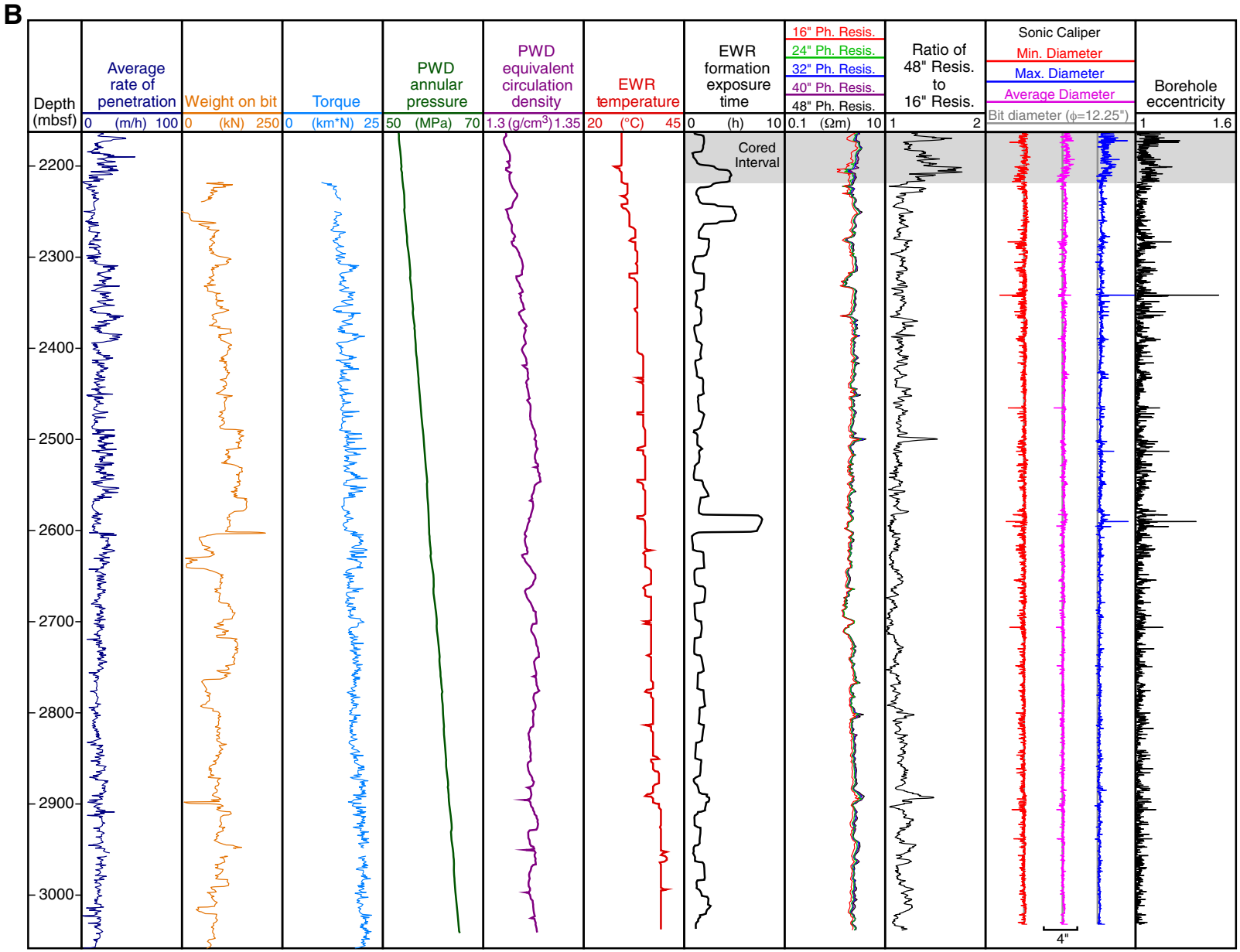

Figure F19. Composite plot of logging while drilling logs, Hole C0002N. Gamma ray (DGRCC), phase (PC), and attenuation (AC) resistivity curves for different sensor spacings (9, 15, 27, and 39 inch). The R09PC and R09AC short-spacing and, to a lesser degree, the R15PC and R15AC exhibit low resistivity values compared to those of the deep readings (R27PC, R39PC, R27AC, and R39PC). The short-spacing receivers record the response of the electromagnetic wave propagation in the mud, and the long-spacing receivers provide a measurement of the formation. Only deep resistivities were used in the geological interpretation.

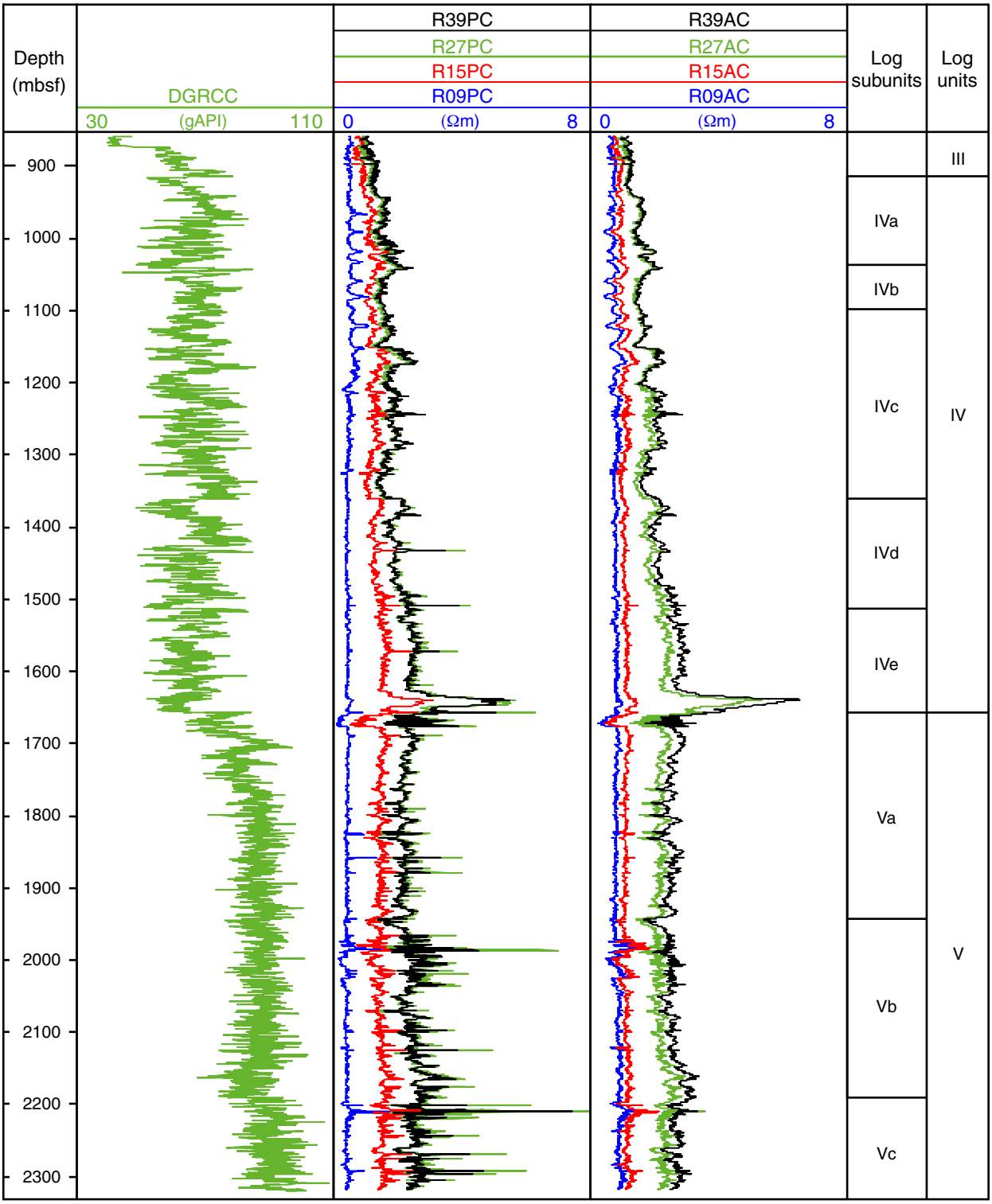

Figure F20. Correlation of logging units and subunits between Holes C0002N and C0002P. Logging units and subunits defined in Hole C0002P were correlated to Hole C0002N based on the gamma ray and resistivity log responses in Hole C0002N. The definition and characterization of units and subunits in Hole C0002P is based on a more complete data set including resistivity images and acoustic logs. Major boundaries and changes in trend or character could be identified and correlated. Gamma ray values in Hole C0002N are higher throughout, which may be an artifact (see "Logging").

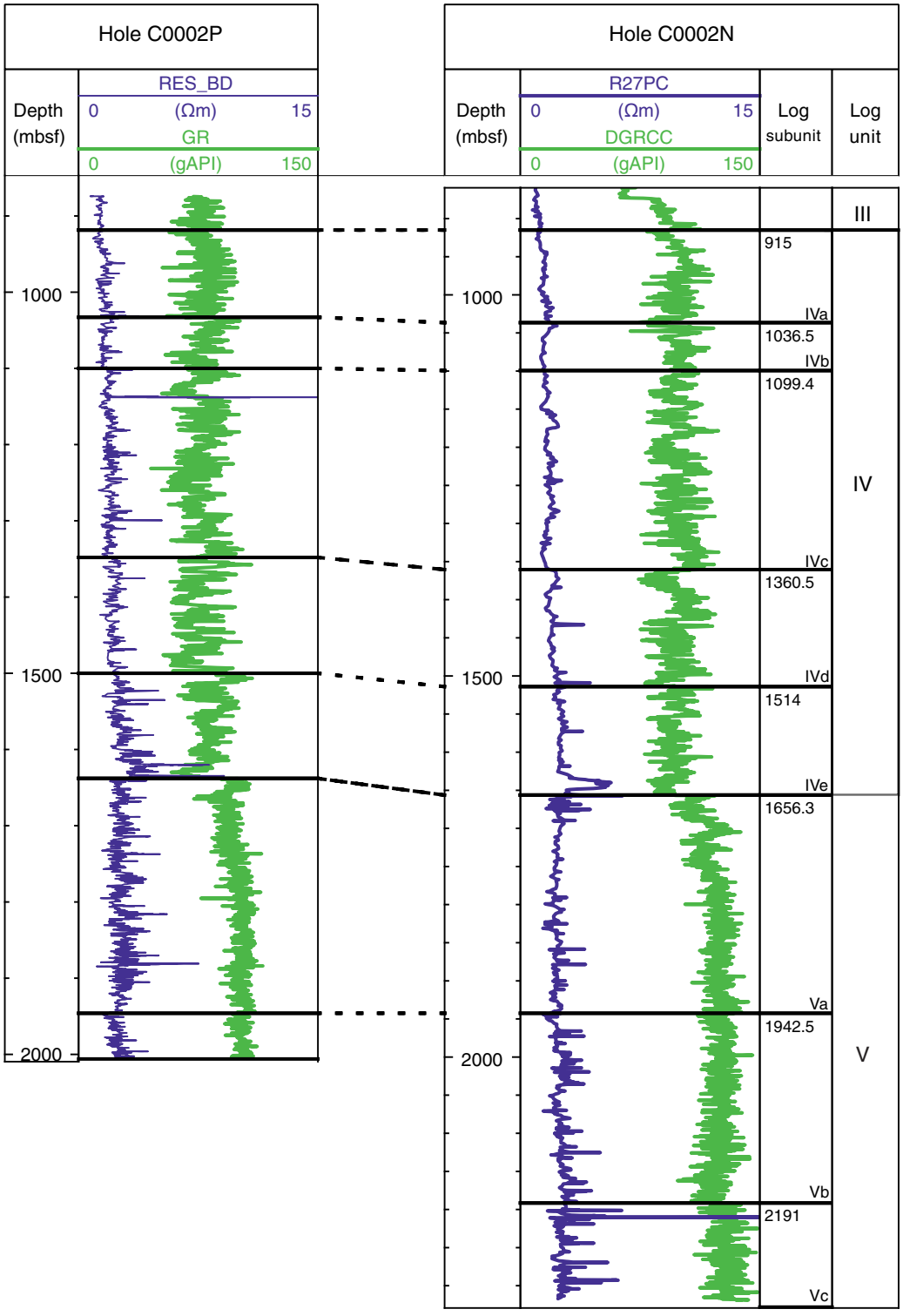

Figure F21. Summary of main logging-while-drilling logs, Hole C0002P. Gamma radioactivity is from the azimuthal gamma ray tool (AGRCC), and compressional slowness is from the X-BAT tool (XBCS). Compressional velocity (XBCS) and 3-phase 2 MHz resistivity measurements are from the electromagnetic wave resistivity tool with different depths of investigation, from shallowest (RH16PC) to deepest (RH48PC). Dotted lines indicate main trends observed on the different logs.

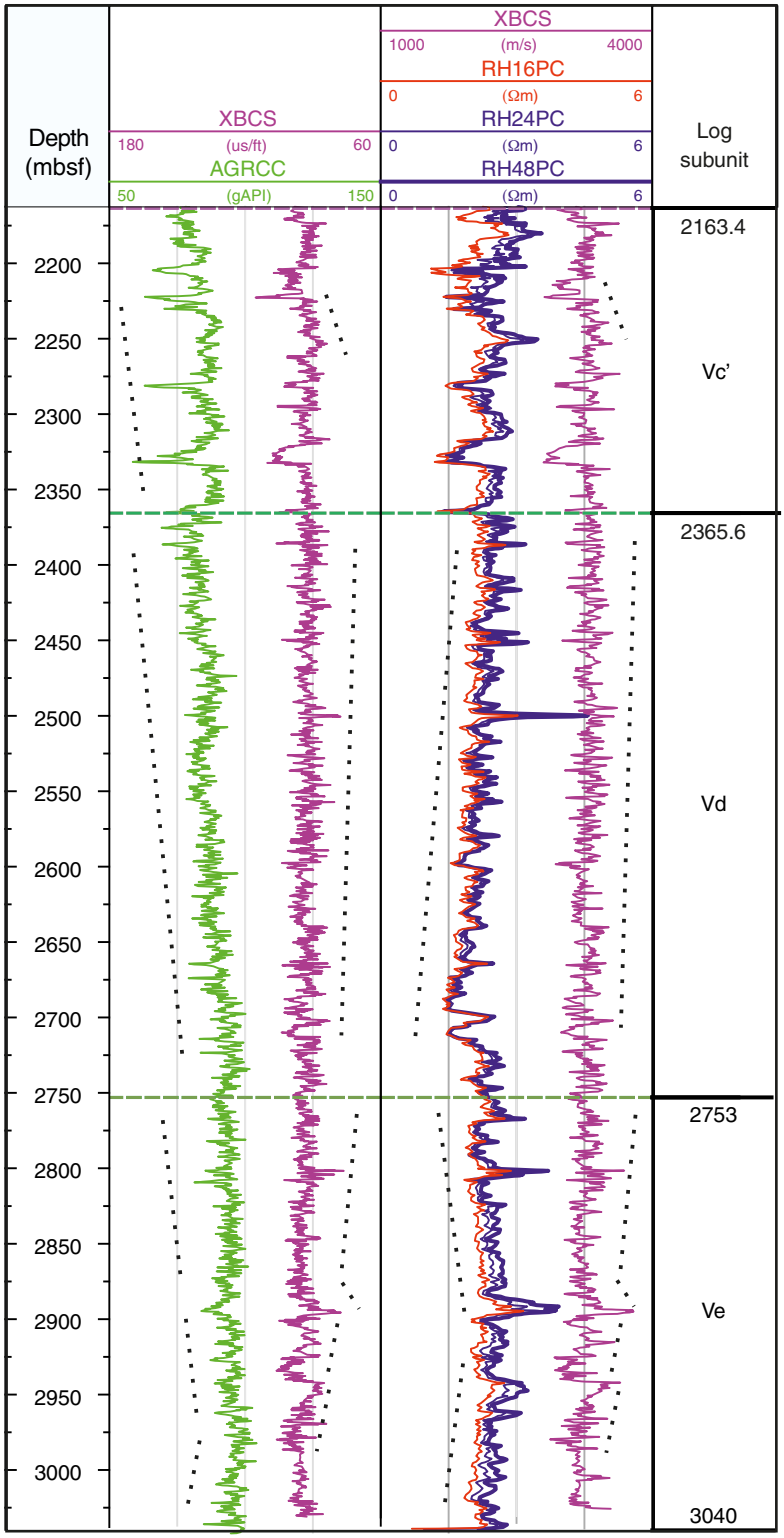

Figure F22. Summary of the preliminary interpretation of azimuthal focused resistivity (AFR) images displayed with velocity, resistivity (RH48PC), and gamma radioactivity (AGRCC). Tadpole plot of downsampled bedding dips (interval = 30 m, step = 15) and shipboard *P*-wave velocity, high-resolution AFR image (static processing), tadpole plot of structures, resistivity, and gamma ray logs.

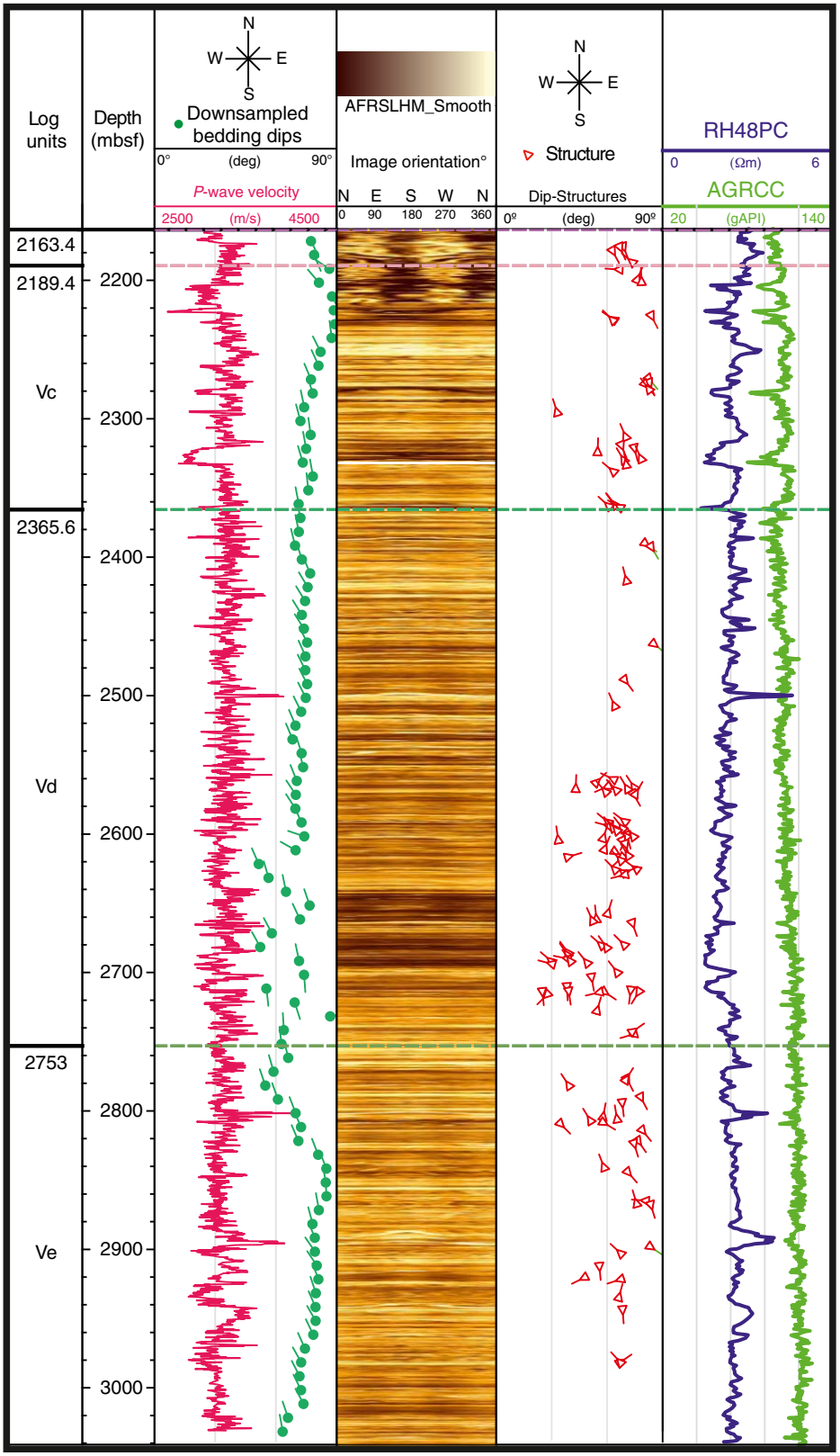

Figure F23. Summary of wellbore failures observed in the resistivity image log shown with the sonic caliper image. AFR = azimuthal focused resistivity.